The role of wind in determining the timing of the spring bloom in the Strait of Georgia

A. Kathleen Collins, Susan E. Allen, and Rich Pawlowicz

Abstract: A coupled biophysical model of the Strait of Georgia (SoG), British Columbia, Canada, has been developed and successfully predicts the timing of the spring phytoplankton bloom. The physical model is a one-dimensional vertical mixing model, using a K-profile parametrization of the boundary layer, forced with high frequency meteorological data. The biological model includes one phytoplankton class (microphytoplankton) and one nutrient source (nitrate). The spring bloom in the SoG occurs when phytoplankton receive enough light that their growth rates exceed their loss rates. The amount of light that the phytoplankton receive is a function of solar radiation and the depth of mixing. The model was used to determine what physical factors are controlling the phytoplankton losses and the light received by the phytoplankton. Wind was found to control the spring bloom arrival time, with strong winds increasing the mixing-layer depth and delaying the bloom. The amount of incoming solar irradiance, through amount of cloud cover, had a secondary effect. The freshwater input (primarily Fraser River discharge) had an insignificant effect on the timing. Increased freshwater flux increases the buoyancy flux and thus decreases the mixing-layer depth but also increases the strength of the estuarine circulation, increasing the advective loss.

Résumé : Nous avons élaboré un modèle biophysique couplé du détroit de Géorgie (SoG), Colombie-Britannique, Canada, qui prédit avec succès le moment de la prolifération printanière du phytoplancton. Le modèle physique est un modèle de brassage vertical unidimensionnel, avec un paramétrage du profil K de la couche limite, forcé par des données météorologiques de haute fréquence. Le modèle biologique comprend une classe de phytoplancton (le microphytoplancton) et une source de nutriments (le nitrate). La prolifération printanière dans le SoG se produit lorsque le phytoplancton reçoit assez de lumière pour que son taux de croissance surpasse son taux de perte. La quantité de lumière reçue par le phytoplancton est fonction de la radiation solaire et de la profondeur du brassage. Le modèle a servi à déterminer quels facteurs physiques contrôlent les pertes du phytoplancton et la lumière reçue par le phytoplancton. Le vent contrôle le moment de l'arrivée de la prolifération printanière; cependant, les vents forts augmentent la profondeur de la couche de mélange et retardent la prolifération. La quantité d'éclairement solaire incident a un effet secondaire selon l'importance de la couverture nuageuse. L'apport d'eau douce (principalement le débit du Fraser) a un effet négligeable sur le calendrier de la prolifération. L'apport accru d'eau douce augmente le flux de flottabilité et diminue ainsi la profondeur de la couche de mélange, mais augmente aussi la force de la circulation dans l'estuaire, accroissant ainsi les pertes par advection.

[Traduit par la Rédaction]

Introduction

The Strait of Georgia (SoG) is a semi-enclosed, deep sea (maximum depth 400 m) located off the coast of mainland British Columbia, Canada (Fig. 1). In the southern SoG, the near-surface physical oceanography is dominated by the Fraser River plume and the estuarine flow it produces (Pawlowicz et al. 2007). The SoG is too large to be considered a classic estuary, but its dynamics are similar to those of smaller fjord estuaries. It is productive (yearly average productivity 1.6 g $C \cdot m^{-2} \cdot day^{-1}$) and, being a temperate sea, has a classic diatom-dominated spring bloom and a weaker fall bloom (R. Pawlowicz, A.R. Sastri, S.E. Allen, D. Cassis, O. Riche, M. Halverson, R. El-Sabaawi, and J.F. Dower, unpublished data). The timing of the spring bloom has been observed to vary interannually by as much as 6 weeks, with blooms as early as February and as late as mid-April (R. Pawlowicz, A.R. Sastri, S.E. Allen, D. Cassis, O. Riche, M. Halverson, R. El-Sabaawi, and J.F. Dower, unpublished data). The timing of the bloom is believed to be influential in the survival of various higher trophic levels, including, for example, Pacific herring (*Clupea pallasi*) and the historically dominant copepod *Neocalanus plumchrus*. The larval stages of Pacific herring have a fixed spawning time (Beamish et al. 2004), which may or may not coincide with the increased food supply associated with the bloom. Nauplii of *N. plumchrus* migrate to the surface in the spring. If the spring bloom is very early, the nauplii can miss the

Received 12 June 2008. Accepted 30 March 2009. Published on the NRC Research Press Web site at cjfas.nrc.ca on 9 September 2009. J20616

Paper handled by Associate Editor Gary Sprules.

A.K. Collins,[1] S.E. Allen,[2] and R. Pawlowicz. Department of Earth and Ocean Sciences, University of British Columbia, 6339 Stores Road, Vancouver, BC V6T 1Z4, Canada.

[1]Present address: Bedford Institute of Oceanography, Fisheries and Oceans Canada, P.O. Box 1006, Dartmouth, NS B2Y 4A2, Canada.
[2]Corresponding author (e-mail: sallen@eos.ubc.ca).

Fig. 1. Study region including sampling stations S3 and S2-2, the Fraser River, Parksville, Vancouver, Halibut Buoy, Sandheads Meteorological Station, and Vancouver International Airport (YVR).

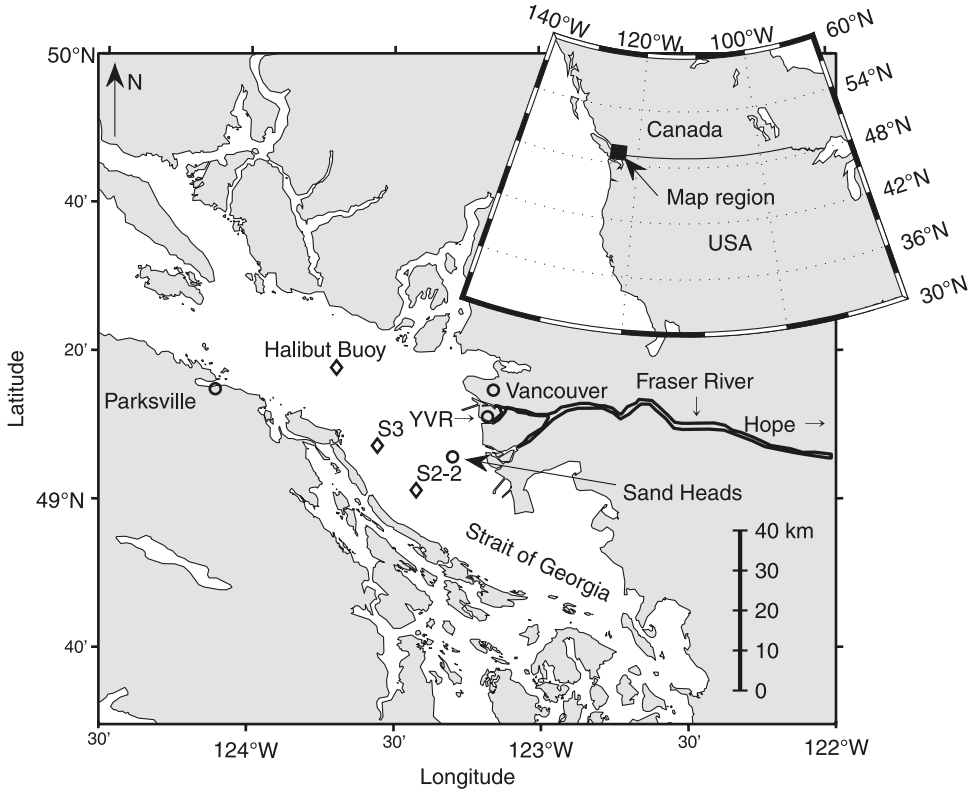

spring bloom and rely solely on postbloom plankton, which are less nutritious (El-Sabaawi et al. 2009). Here we use a numerical model to investigate what processes cause variation in the timing of the spring bloom and develop a simple method for predicting that time.

The spring bloom is a time of rapid accumulation of phytoplankton biomass, which occurs after the relatively low biomass observed in the winter. This accumulation arises because growth rates exceed loss rates for a period of time. We will first discuss factors influencing growth rates and then consider losses. Growth rates can be limited by light or nutrients and retarded by cold temperatures. In the summer, productivity in the SoG can be limited by lack of nitrate (Yin et al. 1997*a*). Other nutrient limitations have not been measured directly, though in some years, silicon is near limiting values towards the end of the spring bloom (R. Pawlowicz, A.R. Sastri, S.E. Allen, D. Cassis, O. Riche, M. Halverson, R. El-Sabaawi, and J.F. Dower, unpublished data). However, in the winter, both these nutrients are well above saturation (R. Pawlowicz, A.R. Sastri, S.E. Allen, D. Cassis, O. Riche, M. Halverson, R. El-Sabaawi, and J.F. Dower, unpublished data), and so phytoplankton growth must be limited by light. Assuming a secondary role for changes in losses, the spring bloom must be initiated by an increase in the net daily light experienced by phytoplankton.

The amount of light that a phytoplankter experiences will be set by a number of factors: (*i*) those that influence the amount of light entering the surface water (length of day, sun angle, amount of cloud in the atmosphere, and surface albedo); (*ii*) those that absorb or reflect light in the water, changing the light extinction coefficient in the water, and (*iii*) the depth of the phytoplankter. The phytoplankton near the surface will always receive the most light, but due to vertical mixing, no phytoplankton is likely to stay at the surface for very long. So a key factor in the amount of light that a phytoplankter receives is the mixing near the surface.

Sverdrup (1953) expressed this effect as critical depth, which was compared with the mixed-layer depth. If critical depth, defined as the depth at which integrated growth equals the integrated respiration, is deeper than the mixed-layer depth, then net growth and a possible bloom are expected. However, the mixed layer, defined as a region near the surface that is well mixed with respect to salinity and temperature, is not always equivalent to the mixing layer, i.e., the layer that is actively mixing. Results from cases in which the mixing layer is shallower than a residual mixed layer can lead to blooms even where the mixed layer is deeper than the critical depth (Huisman et al. 1999). In the SoG, we have the opposite effect. Mixing is occurring without homogenization of properties because there is a significant buoyancy flux into the upper water column. This effect has been seen previously in other regions and authors have assumed that active mixing is occurring down to the strong halocline (Erga and Heimdal 1984). The terminology of a mixing layer as opposed to a mixed layer is carefully used, for example, in Parsons et al. (1984). Mixing-layer depth is a function of processes adding kinetic turbulent energy, which deepens and attempts to homogenize the layer (wind, cooling), and processes adding potential energy, which shallows and attempts to restratify the layer (freshwater influx, warming).

Losses to the phytoplankton biomass can occur due to ad-

vection, sinking, grazing, and viral lysis. A sharp decrease in the loss rate could generate a spring bloom. However, advection changes slowly in the SoG, and the remaining terms are more likely to change in response to the accumulation of biomass rather than causing it. The estuarine circulation in the SoG causes vertical entrainment of deeper water into the surface layer and horizontal advective loss. The strength of this circulation is determined by the freshwater flux into the SoG, which varies on time scales of weeks.

Thus we expect a central role in the timing of the spring bloom for the amount of light reaching the SoG and for the mixing-layer depth and a secondary role for the advective loss. In this paper, we will investigate the role of the principal physical forcings on the SoG, which vary interannually (wind, freshwater flux, and cloud fraction). We wish to determine which of these physical forcings, within the observed variation of the forcing, most strongly influence the timing of the spring bloom.

To directly observe mixing-layer depth, one can use various instantaneous turbulence measurements, but it is much harder to maintain measurements over an extended period, and unlike mixed depth, which is due to the integrative effects of mixing, mixing-layer depth varies rapidly. Here, the depth of the mixing layer will be calculated using a turbulence closure model designed for the surface ocean (Large et al. 1994). Recent one-dimensional (1D) models have considered the timing of the spring bloom in Prince William Sound (Eslinger et al. 2001) and the Bering Sea (Jin et al. 2006). In both cases, the phytoplankton is light-limited and the initiation of the bloom is due to reduced mixing and increased stratification. In the Bering Sea, ice is usually a controlling factor, but in ice-free years, Jin et al. (2006) showed that wind mixing and thermal stratification controlled the mixing-layer depth and thus the timing of the bloom. They were limited in their investigation of interannual variations as they had only one year of ice-free data. Using three years of data in Prince William Sound, Eslinger et al. (2001) showed that, again, wind mixing controlled the mixing-layer depth and the timing of the spring bloom. In both these regions, thermal stratification dominates over salinity stratification; whereas in the SoG, salinity stratification dominates due to the large freshwater fluxes. For the SoG, it has therefore been postulated that the beginning of the large freshwater flux due to snowmelt (the freshet) is necessary for the mixing layer to shallow and the bloom to begin (Yin et al. 1997*b*).

Recently, an extensive set of physical and biological data has been collected for the southern portion of the Strait. These data include meteorological parameters, hydrological data, and a vast set of hydrographic and biological data collected as part of the STRATOGEM (Strait of Georgia Ecosystem Modeling) program, including three years of monthly or more frequent surveys and four years of continuous data collection from the ferries crossing the SoG (Pawlowicz et al. 2007). The high quality and high frequency data from the STRATOGEM project provide an opportunity to develop a coupled biophysical model that includes high frequency (hourly) variations of atmospheric forcing. In the work reported here, the biological model is optimized to find the timing of the spring bloom. The spring bloom is initiated as light limitation lifts, leading to a diatom bloom that is terminated by nitrate exhaustion. Thus our biological model only includes one nutrient type (nitrate) and one phytoplankton (a diatom).

We have chosen to use a high resolution 1D (vertical) coupled biophysical model to correctly model the surface mixing layer. Spatial variations in bloom timing are relatively small: data from the ferries crossing the SoG show that the spring bloom occurs nearly simultaneously (within 3 days) across the Strait. Survey data show that although patchy, chlorophyll distributions are reasonably similar throughout the southern Strait. Two-layer models of the SoG (St. John et al. 1993; Li et al. 2000) cannot capture the details near the surface, and 3D models of the SoG (Masson and Cummins 2004) have limited resolution near the surface. The knowledge from previous studies and the high quality data collected as part of STRATOGEM allow us to parametrize the necessary 2D physical processes and tune the 1D model to correctly represent the SoG physics. We use physical dynamical understanding to ensure that these parametrizations have correct properties beyond the observed values. This then provides a simple, fast-running model that we can use both in interpolative mode for the observed years and in extrapolative mode for years without data and for hypothetical physical forcings. This latter facility allows us to vary wind speed, cloud fraction, and freshwater flux individually to determine their separate impacts on the timing of the spring bloom.

Material and methods

Site

The Fraser River is the largest river in British Columbia and contributes 60% to 70% of the freshwater entering the Strait (Herlinveaux and Tully 1961; Pawlowicz et al. 2007). Flow is relatively low during the winter months (average winter flow at Hope, 150 km upstream, is 8.5×10^2 $m^3 \cdot s^{-1}$ (Environment Canada 2006)), begins to increase in April–May, and then peaks in June when the mountain snowpack melts; this is termed the freshet (average freshet at Hope is 8×10^3 $m^3 \cdot s^{-1}$).

Winds are generally weak in the SoG compared with in the open coastal ocean; average wind speed is 5.2 $m \cdot s^{-1}$ between 2001 and 2005 (Environment Canada 2002) at Sandheads (Fig. 1). The winds follow a seasonal pattern, with the strongest winds occurring during winter storms and very weak wind conditions occurring during high pressure periods in the summer. Cloud cover in the SoG region typically follows a pattern of obscured skies throughout much of the winter months and clear skies during the summer.

The biological community in the SoG is characterized by a phytoplankton bloom of average magnitude 30 mg $Chl \cdot m^{-3}$ that typically occurs in the early spring, followed by an increase in zooplankton grazers and nutrient depletion (Harrison et al. 1983). The spring bloom is initially composed of the chain-forming diatom *Thalassiosira* spp. and progresses with the explosion of *Skeletonema costatum*, with the diatom *Chaetoceros convolutus* blooming more slowly (Harrison et al. 1983; Hobson and McQuoid 1997). Ammonium and urea concentrations are low in the SoG (NH_4^+ concentrations of 0.5 to 2 $\mu mol \cdot L^{-1}$ directly after the spring bloom (Yin et al. 1996)) compared with nitrate, which is

abundant (30 μmol·L^{-1}; R. Pawlowicz, A.R. Sastri, S.E. Allen, D. Cassis, O. Riche, M. Halverson, R. El-Sabaawi, and J.F. Dower, unpublished data) and is an important nutrient source for phytoplankton throughout the year and probably the primary nutrient during the bloom (Harrison et al. 1983). Average yearly f ratios have been estimated at 0.3–0.4 (Mackas and Harrison 1997) and, more recently, 0.5 (R. Pawlowicz, A.R. Sastri, S.E. Allen, D. Cassis, O. Riche, M. Halverson, R. El-Sabaawi, and J.F. Dower, unpublished data). The surface macrozooplankton community in the SoG is mainly composed of copepods and was historically dominated by the large calanoid copepod *Neocalanus plumchrus* (Harrison et al. 1983). *Neocalanus plumchrus* depends on phytoplankton biomass for survival and growth (Kobari and Ikeda 2001) and is perhaps a substantial food source for salmon (Parsons et al. 1984).

Data

The field data used in this study were collected over four years at nine stations in the SoG. The nominal location being modeled is station S3 (Fig. 1). Sampling took place approximately once per month and more frequently during the spring phytoplankton bloom. Casts were taken with a conductivity–temperature–depth (CTD) sensor; variables recorded at each station included chlorophyll fluorescence, photosynthetically active radiation (I_{PAR}), temperature, and salinity. Nitrate, chlorophyll, salinity, oxygen, and taxonomy samples were taken at depths of 0, 5, 10, and 30 m. The chlorophyll samples were filtered and size-fractionated, and the largest fraction (>20 μm) was used for model comparison. Continuous surface salinity, temperature, and chlorophyll fluorescence data are available from a sampling program aboard several BC Ferries vessels, one of which passes near station S3. Fluorescence data from within a 2 min latitude by× 2 min longitude box centered on S3 were used to compare with model output.

Wind speed and direction were obtained from Environment Canada's weather station at Sandheads CS, an exposed site at the edge of the mud flats of the Fraser River delta (all locations, Fig. 1) (Environment Canada 2002). Other meteorological data not available from the automatic station at Sandheads (hourly humidity, air temperature, cloud fraction) were obtained from Environment Canada's weather station at the Vancouver International Airport (Environment Canada 2002). Fraser River flow is measured daily at Hope, BC, 150 km upstream of where the river enters the Strait, and Englishman River flow is measured daily at Parksville, BC (Environment Canada 2006). Downward shortwave radiation data measured by the UBC Department of Agroecology was used for the parametrization of the cloud model that will be described in the next section. Irradiance data from Halibut Bank Buoy were used to verify the cloud model.

The physical model

The physical model used is an adapted version of the K-profile parametrization (KPP) nonlocal boundary-layer model (Large et al. 1994). The model represents mixing due to turbulent vertical velocities of unresolved eddies and calculates numerical values for the horizontal velocities, temperature, salinity, and diffusivity in time and space. The fine vertical grid resolution available from a 1D model enables the careful evaluation of near-surface mixing and its importance on phytoplankton growth; the speed of calculations allows for many model runs.

We will neglect the tides in the model. Tides in the central SoG are of maximum velocity 0.5 m·s^{-1} but contribute little mixing to the system because of the depth of the Strait (200–400 m) (Thomson 1994). This is in direct contrast to the strong tidal mixing that occurs to the south and north of the SoG in narrow, shallow, and complicated channels. In the SoG, tidal excursions are on the order of 10 km, which is small compared with the size of the central SoG and so the advective role of the tides is not a dominant factor because variations within the tidal excursion are small.

The KPP model has been incorporated into a number of large 3D models (ROMS, e.g., Durski et al. (2004); HYCOM, e.g., Chassignet et al. (2003); MITgcm, e.g., Campin et al. (2008)). Some results show stronger mixing for the KPP model than for the Mellor–Yamada 2.5 turbulence closure scheme (Durski et al. 2004) that had been used by Denman and Peña (2002), for example, to model phytoplankton cycles in the Northeast Pacific Ocean. Other results show weaker mixing and suggest better agreement with turbulence measurements (Kettle 2005). KPP and Mellor–Yamada 2.5 models are the most commonly used turbulent parametrizations.

To use any 1D mixing models in the SoG requires incorporation of additional processes. The SoG has a number of important horizontal processes, including the estuarine circulation and baroclinic pressure gradients. These processes must be parametrized in the physical model, are additions to the standard KPP model, and are explained in detail below.

The equations for across-strait and along-strait velocity, salinity, and temperature can be represented as, respectively,

$$(1a)\qquad \frac{\partial u}{\partial t} - fv = \underline{-\frac{1}{\rho_0}\frac{\partial p}{\partial x} - \frac{\partial}{\partial z}(w_e u)} + \mathcal{V}(u)$$

$$(1b)\qquad \frac{\partial v}{\partial t} + fu = \underline{-\frac{1}{\rho_0}\frac{\partial p}{\partial y} - \frac{\partial}{\partial z}(w_e v)} + \mathcal{V}(v)$$

$$(1c)\qquad \frac{\partial S}{\partial t} = \underline{-\frac{\partial}{\partial z}(w_e S) + J_s \exp(\gamma z)} + \mathcal{V}(S)$$

$$(1d)\qquad \frac{\partial T}{\partial t} = \underline{-\frac{\partial}{\partial z}(w_e T)} + \frac{I_{TOTAL}(z)}{c_p\ \rho(z)} + \mathcal{V}(T)$$

where u and v are the across- and along-strait velocities, respectively, S is salinity, T is temperature, t is time, x and y are along- and across-strait distances, respectively, z is vertically upward distance starting at the sea surface (so all z values are negative), f is the Coriolis parameter, $\mathcal{V}$ is the mixing prescribed by the KPP model (Large et al. 1994), p is the baroclinic pressure, ρ is the density of water, ρ_0 is a constant reference density, c_p is the specific heat at constant pressure, w_e is a vertical upwelling flux, J_s is an added freshwater flux, $1/\gamma$ is the scale depth of the freshwater flux, and I_{TOTAL} is the incoming shortwave radiation. Surface boundary conditions for the momentum equations include wind stress, and those for the temperature include the longwave radiation balance and the sensible and latent heat

Fig. 2. (*a*) Fraser River (left axis) and Englishman River (right axis) flow for January 2002 – June 2005. (*b*) Salinity fit based on Fraser River and Englishman River flow data and observations of surface salinity at station S3.

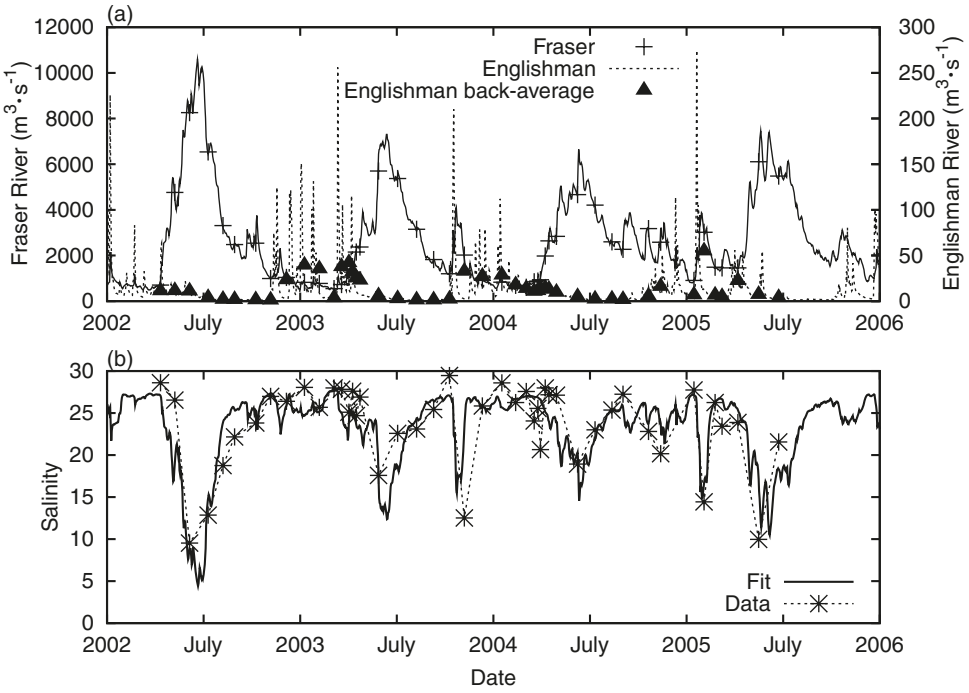

flux. The underlined terms are those additional to the standard KPP model, and they and the incoming shortwave radiation are discussed in the next three subsections.

Estuarine flow

The effect of the estuarine flow is seen in the two underlined terms of the salinity equation (eq. 1*c*). Estuarine flow has two effects. First, the freshwater flow into the Strait keeps the surface relatively fresh and is the main stratifying influence (J_s). In the model, freshwater is added to the surface layer based on a parametrization of total freshwater flow into the Strait. Second, estuarine entrainment from the deeper water into the surface layer causes a slow upwelling of the water column (w_e).

Empirically, we find that the surface salinity at station S3 is well correlated with the input of freshwater into the SoG. This input is composed of the Fraser River (with sources in the interior of British Columbia) and a number of smaller rivers that drain coastal areas. Most of these are not measured, but we assume that their effect will be similar to that of the Englishman River. We model the total freshwater flux as

$$(2a) \qquad Q_T = Q_F + a_E Q_E$$

where Q_T is the effective total freshwater flux, Q_F is the Fraser River flux, a_E = 55.0, and Q_E is a 20-day back-average of the Englishman River flux (Fig. 2*a*). Then we model the surface salinity at station S3 as

$$(2b) \qquad S_{surface} = S_D \frac{\exp(-Q_T/\alpha_f)}{\gamma_f + \exp(-Q_T/\alpha_f)}$$

where S_D = 30.0, α_f = 2440 m^3·s^{-1}, and γ_f = 0.0633 (subscript "f" refers to freshwater flux) (Fig. 2*b*); R^2 = 0.61. This allows us to interpolate the observed salinities at station S3 to daily resolution.

Next, to force the surface salinities in the model to these observations, we add a forcing term:

$$(3) \qquad J_s \exp(\gamma z) = F_w S_0 \left(\frac{Q_T}{\overline{Q}}\right)^{\sigma_s} \exp\left(\frac{z}{a_h h_m}\right)$$

where F_w = 3.0 × 10^{-6}·s^{-1}, S_0 is the mixed-layer salinity at the previous time step, $\overline{Q}$ = 3624 m^3·s^{-1}, σ_s = 1.12, a_h = 3.5, and h_m is the mixing-layer depth determined by the KPP model. The constants F_w, σ_t, and a_h were selected to match the model salinity to the interpolated observed salinity; see the Results section. We see that the scale depth over which the freshwater flux impacts the water column is $1/\gamma = a_h h_m$.

Vertical advection (upwelling) is assumed to be dominated by the estuarine circulation. The vertical velocity was determined using a similarity solution fitted to observations of salinity at stations S3 and S2-2, Knudson relations, and a force balance between the estuarine pressure gradient and the turbulent momentum mixing (see Appendix A):

$$(4) \qquad w_e = w_* \left[2.72 \frac{Q_T}{\overline{Q}} \exp\left(\frac{-Q_T}{\overline{Q}}\right)\right] \left[1 - \left(1 + \frac{z}{2.5\, d}\right)^2\right]$$

where w_* = 2.5 × 10^{-5} m·s^{-1}, $\overline{Q}$ = 3624 m^3·s^{-1}, and d = 11.7 m is the average depth at which the cumulative freshwater reaches 67% of its surface value at station S3. Although complex, the primary purpose of these parameterizations is to ensure that the physical parameters of the water column are realistically represented not only for years with observations, but also for years without data and for hypothetical physical forcings.

This vertical velocity controls the vertical advection of salt (eq. 1*c*), temperature (eq. 1*d*), momentum (eqs. 1*a* and

Fig. 3. Sketch of the vertical velocity field as a function of depth (vertical arrows) and the resulting detrained flux of water (horizontal arrows).

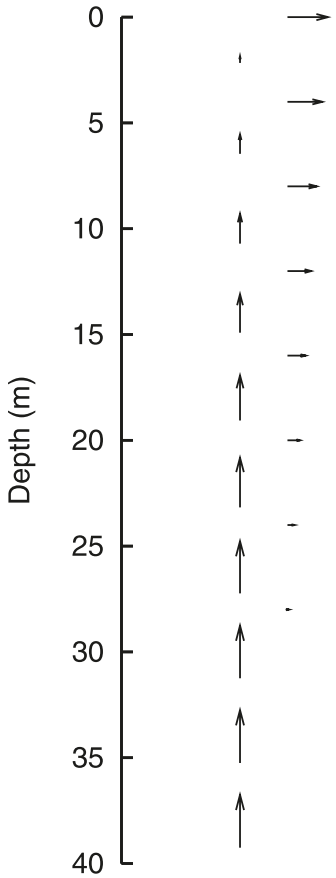

1*b*), nitrate, and phytoplankton. As the vertical velocity has convergence (that is, it is stronger at depth than near the surface), detrainment (removal) of these properties, as well as water, occurs throughout the depth of the model (Fig. 3). This advective loss is a significant loss term for the phytoplankton in winter. The vertical velocity at depth is a function of the river flow (eq. 4); for the river flows observed, this velocity is usually between 1.8 and 2.5 $\times$ 10^{-5} m·s^{-1}, only rarely drops below 1.6 $\times$ 10^{-5} m·s^{-1}, and never goes below 0.95 $\times$ 10^{-5} m·s^{-1}.

Baroclinic pressure gradients

In the open ocean, flow in a given direction in a given layer between isopycnals can continue in a single direction without particular consequences. In a constricted basin it causes an accumulation of mass within that layer downstream and a corresponding baroclinic pressure gradient against the flow. These pressure gradients appear in the momentum eqs. 1*a* and 1*b*.

To include this pressure gradient, it is assumed that (*a*) the basin is shaped like an ellipse with nearly vertical sides; (*b*) station S3 is located in the exact center of the basin; and (*c*) the basin is initially uniformly stratified. A flow in a given isopycnic layer will cause a thickening (thinning) of that layer downstream (upstream):

Fig. 4. Illustration of the scheme used to solve for the *x* and *y* baroclinic pressure gradients. This shows the scheme in one dimension, the same theory applies for two dimensions. Broken lines denote undisturbed isopycnals at the grid spacing, and solid lines denote the instantaneous isopycnals. Flow from left to right, as illustrated in the top layer, causes the layer to thicken to the right, thereby reducing the baroclinic pressure below.

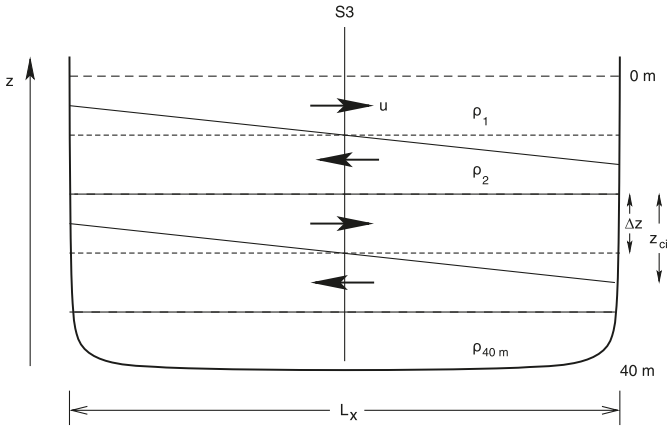

$$(5) \qquad z_{ci}^{x} = \int \frac{U_i \mathrm{d}t}{L_x/2} + \Delta z$$

where U_i is the baroclinic velocity $u_i - \langle u_i \rangle$ in the ith layer with $i = 1$ being the top layer, $\langle\ \rangle$ implies the vertical average, L_x is the width of the ellipse, Δz is the undisturbed thickness of the layer, and z_{ci}^{x} is the thickness at the positive x boundary of the ellipse (Fig. 4). The thickness at the positive y boundary is found similarly.

These tilted isobars cause baroclinic pressure gradients at z_i of

$$(6) \qquad \frac{\partial p_i}{\partial x} = \frac{g}{\rho_0 L_x}\left\{\sum_{j=1}^{k}\rho_j z_{cj} + \rho_{k+1}\left(\sum_{j=1}^{k} z_{cj} - |z_i|\right) - \sum_{j=1}^{i}\rho_j \Delta z\right\}$$

where k is the last full layer just above z_i and the expression inside the parentheses is the fraction of the k+1 layer above z_i. In addition, g is the acceleration due to gravity, ρ_i is the density in the ith layer, and ρ_0 is a constant reference density. The calculation is similar for the pressure gradient in y. These are the pressure gradient terms used in eqs. 1*a* and 1*b*. We use L_x = 60 km and L_y = 240 km, with the ellipse oriented with its major axis northwest–southeast with its northwest end 55°E of North.

Light

The physical model incorporates light in three parts, beginning with a cloud model that filters light from the sun, an albedo, and parametrizations for the deposition of photosynthetically active radiation and for the total light spectrum that is available for heat. All calculations for light use units of W·m^{-2}. To compare I_{PAR} with field data measured in μE·m^{-2}·s^{-1}, these units are converted to W·m^{-2} using a conversion factor of 0.2174, recommended by the I_{PAR} sensor manufacturer (Biospherical Instruments Inc.). This is based on a quanta-to-Watt ratio of 2.77 $\times$ 10^{18} quanta·s^{-1}·W^{-1}.

Table 1. Parameters used in the biological model.

Symbol	Parameter	Value	Source
R_{max} (T_{ref})	Maximum growth rate (24 h)	2.16·day^{-1}	Durbin (1974) and Hitchcock (1980)
T_{ref}	Reference temperature	10 °C	
I_{opt}	Optimal light level	38.4 W·m^{-2}	Fit to Steele (1962) and Durbin (1974)
α_T	Temperature effect slope	0.07 °C	Eppley (1972)
κ	Half-saturation, nitrate	0.5 μmol·L^{-1}	Falkowski (1975)
W_1	Sinking rate, nutrient replete	0.5 m·day^{-1}	Cugier et al. (2005)
W_2	Sinking rate, nutrient depleted	1.2 m·day^{-1}	Cugier et al. (2005)
R_M (T_{ref})	Mortality	0.1·day^{-1}	Spitz et al. (2003)
	Maximum temperature for growth	18 °C	Durbin (1974)
	Range of decrease due to temperature	8 °C	
κ_p	Half-saturation, mesozooplankton on diatoms	0.5 μmol N·L^{-1}	From data
$\Upsilon(T_{ref})$	Maximum ingestion, mesozooplankton	0.6·day^{-1}	Cugier et al. (2005)
Z_w	Winter concentration, zooplankton	0.168 μmol N·L^{-1}	Tuned

The methodology of a cloud model for the open seas of the North Atlantic Ocean (Dobson and Smith 1988) was followed to develop a new cloud model for the SoG using shortwave radiation obtained from the Department of Agroecology Science at UBC (R. Ketler, Department of Agroecology, University of British Columbia, Vancouver, British Columbia, personal communication, 2005).

An albedo value of 18% was calculated for the SoG by measuring I_{PAR} just above and just below the sea surface at nine stations on 11 November 2004. Albedo varies from ~0.03 to 0.4 with season, sea roughness, and water clarity (Jin et al. 2004), so a value of 18% for the productive and turbid SoG is appropriately higher than the open-ocean value of 6% used by Large et al. (1994); we include albedo as a constant value following Large et al. (1994).

The depth distribution of photosynthetically active radiation (I_{PAR}, 400–700 nm) requires a distinction from the total light (300–2500 nm). Integrating the whole light spectrum (Jerlov 1976), we find that 44% is in the photosynthetically available range. Therefore surface irradiance ($I_{PAR}(0\,m)$) is calculated in the model as 44% of the total nonreflected light. Analysis of the SoG irradiance data showed that I_{PAR} follows an exponential decay:

$$I_{PAR}(z) = I_{PAR}(0\,m)\exp(K_{PAR}z) \tag{7}$$

where K_{PAR} is the attenuation coefficient, which is unknown. A parametrization for K_{PAR} will provide the model with an irradiance profile.

Attenuation (K_{PAR}) of light depends on the amount of particulate matter in the water, including organic material such as phytoplankton and inorganic material such as sediment transported by the Fraser River. An empirical relationship between measured light and the phytoplankton quantity in the water (measured from chlorophyll P_c) and Fraser River flow (Q_F) was found to give

$$K_{PAR}(z) = \alpha_\ell + \beta_\ell \overline{P}^{0.665} + \left[\gamma_\ell \left(\frac{Q_F}{\overline{Q}}\right)^{\sigma_\ell} + \theta_\ell\right]\exp\left(\frac{z}{d_\ell}\right) \tag{8}$$

where the exponent of 0.665 on $\overline{P}$ follows Ménesguen et al. (1995) and $\overline{P} = P_c/(1\,mg\,Chl\cdot m^{-3})$. The fit gave α_ℓ = 0.0910·m^{-1}, β_ℓ = 0.0289·m^{-1}, γ_ℓ = 0.00986·m^{-1}, θ_ℓ = 0.445·m^{-1}, and d_ℓ = 2.56 m. The large exponent on the river flow reflects the fact that young river water (less than 1 day old) only reaches station S3 under strong flow conditions.

The fit is done on the light decrease over 1 m steps for 45 PAR profiles and has R^2 = 0.77. It dictates that as particulate matter in the water column (river sediment or phytoplankton) increases, K_{PAR} increases and light is absorbed closer to the surface because there is more matter to absorb it.

The distribution of total light in the water to calculate the nonturbulent heat flux profile is taken from the Jerlov (1976) water classification system, which provides data on the distribution of light with depth; this distribution follows a double exponential decay. For each of Jerlov's five coastal water types, two attenuation coefficients, K_1 and K_2, are estimated. The K_1 and K_2 values are fit separately to the theoretical K_{PAR} values given by Jerlov for each water type, giving us an expression for each of the attenuation coefficients:

$$K_1 = 0.81K_{PAR} + 1.18\,m^{-1} \tag{9a}$$

$$K_2 = 0.82K_{PAR} - 0.088\,m^{-1} \tag{9b}$$

The fits have R^2 = 0.94 and 0.97, respectively. Equations 9*a* and 9*b* are solved during model computations using the value of K_{PAR} (eq. 8). The total light profile can then be generated by integrating

$$\frac{\partial I_1}{\partial z} = K_1 I_1 \qquad \frac{\partial I_2}{\partial z} = K_2 I_2 \tag{10}$$

using initial conditions

$$I_1(0\,m) = 0.70I(0\,m) \qquad I_2(0\,m) = 0.30I(0\,m) \tag{11}$$

based on eqs. 8, 9*a*, 9*b*, and I(0 m) and where the values 70% and 30% were determined empirically. The value $I_{TOTAL} = I_1 + I_2$ is used for the shortwave radiation in eq. 1*d*.

Wind

Wind speed and direction are measured at a height of 10 m at Sandheads Meteorological Station (Fig. 1) and are transformed from wind speed and direction into meridional (u) and zonal (v) components and rotated to 55°NW to be aligned with the major axis of the SoG. Wind stress is calculated following Large and Pond (1982).

Bottom boundaries

The profile salinity and temperature data at 40 m was fit to constant, seasonal, and bi-seasonal components. The bottle nitrate data at 30 m was averaged and used for the 40 m values as nitrate below 30 m was found to be nearly constant at other stations in the Strait.

The biological model

The objective of the SoG biological model, when coupled with the physical model, is to predict the timing of the spring phytoplankton bloom. The growth rate of phytoplankton and rate of change of nutrient concentration are calculated based on Jeffery (2002), with only one size class of phytoplankton (P) included (microphytoplankton, >20 μm) and nitrate (N) as the sole nutrient modeled. Although phytoplankton use ammonium during the spring bloom, as evidenced by the f ratios, the amount of ammonium available at any time is small and inclusion of ammonium in the model makes no substantial changes to the spring bloom timing and only slightly increases its magnitude. We use the simplest possible model for the spring bloom because the addition of complexity to a model requires the use of more parameters, and in general, biological parameters are poorly constrained. Predictive capability often decreases with model complexity, particularly if the model is only to be used in a single region (e.g., Friedrichs et al. 2006).

All units in the biological model are nitrogen atom concentrations. The phytoplankton and nitrate equations are

$$(12a)\qquad \frac{\partial P}{\partial t} = \left\{ \min[u_c(I_{PAR}), u_n(N)] - R_m - \Upsilon \frac{Z(t,z)}{\kappa_P + P} \right\} P + \frac{\partial}{\partial z}(w_s P) - \frac{\partial}{\partial z}(w_e P) + \mathcal{V}(P)$$

$$(12b)\qquad \frac{\partial N}{\partial t} = -\left\{ \min[u_c(I_{PAR}), u_n(N)] \right\} P - \frac{\partial}{\partial z}(w_e N) + \mathcal{V}(N)$$

where P is the phytoplankton concentration, N is the nitrate concentration, u_c is the growth based on light limitation, u_n is the growth based on nitrate limitation, R_m is the rate of natural mortality, Υ is the maximum ingestion of phytoplankton by zooplankton, Z is the zooplankton concentration, κ_p is the half-saturation for zooplankton grazing, and w_s is the sinking rate of the phytoplankton (positive downward). The last two terms in each equation are, respectively, the estuarine advective loss and the turbulent diffusion determined by the physical model. Further advection terms, due to horizontal currents, cannot easily be incorporated into the 1D model and are neglected as chlorophyll and nitrate distributions are similar throughout the southern Strait.

The values for the biological parameters are provided (Table 1). Each of the biological terms in the two equations will be described below after initialization is discussed. The biological model is a simplified version of the standard NPZD models with origins back to Fasham et al. (1990). The formulation for the nutrient limitation term, the use of a minimum function, and the linear natural mortality are standard formulations for NPZD-type biological models (e.g., Denman and Peña 2002; Cugier et al. 2005). The light limitation term used here is a fit for a particular phytoplankton species, whereas most models use a more general form. We choose a Holling type-II grazing term similar to the Ivlev function used by Cugier et al. (2005), whereas Denman and Peña (2002) use a Holling type-III term.

Initialization

The phytoplankton in the model is initialized using profile fluorescence measurements, which are converted from mg Chl·m^{-3} to μmol N·L^{-1} using a conversion factor of 1.5:1. This ratio was estimated by plotting chlorophyll versus nitrate in the rapid growth time of the spring bloom. It is slightly smaller than, but on order of, the value 2.2 estimated for the Oregon Shelf (Dickson and Wheeler 1995). Ratios of chlorophyll to nitrate vary strongly depending on the health of the phytoplankton. Values at the peak of a bloom can be very high, with lower values especially during nitrate depletion (Parsons et al. 1984). Nutrients are initialized using sampled nitrate bottle data. The data from the bottles (0, 5, 10, and 30 m) is interpolated at 0.5 m intervals to match the grid spacing of the physical model. Nitrate concentrations between depths of 30 m and 40 m are assumed to be constant; this is consistent with observations at other stations in the Strait at which bottle samples were taken at greater depths.

Phytoplankton growth

Phytoplankton growth depends on the availability of light and nutrients and is calculated as a function of whichever is minimum. When nutrients are not limiting, phytoplankton growth depends on light availability:

$$(13)\qquad u_c = R_{max}(T)\left[1 - \exp\left(\frac{-I_{PAR}}{0.67 I_{opt}}\right)\right]\left[1.8\exp\left(\frac{-I_{PAR}}{2.7 I_{opt}}\right)\right]$$

where I_{opt} is the optimum light intensity and $R_{max}(T)$ is the maximum growth rate. The coefficients were chosen to give a Steeles-like shape for low light (Steele 1962) and to fit experimental light curves for *Thalassiosira nordenskioldii* (Durbin 1974) at high light.

When light is not limiting, phytoplankton growth depends on nutrient availability:

$$(14)\qquad u_n = R_{max}(T)\frac{N}{\kappa + N}$$

where κ is the half-saturation constant for nitrate (N).

The maximum growth value, R_{max}, for *Thalassiosira nordenskioldii* was measured as 1.4·day^{-1} and 1.0·day^{-1} at 10 °C for a 12 h light – 12 h dark cycle (Hitchcock 1980; Durbin 1974, respectively). The value used in the model (1.06·day^{-1}) was between these values. Sensitivity to this choice is discussed under model limitations in the Discussion.

Table 2. Model runs used to predict the spring blooms of 2002, 2003, 2004, and 2005 with their observed and modeled peak bloom dates.

Run	Start date	End date	Observed bloom	Modeled bloom
R1	20 September 2001	1 November 2002	1 April 2002	30 March 2002
R2	8 October 2002	1 November 2003	27–30 March 2003	27 March 2003
R3	9 October 2003	1 November 2004	17 March 2004	21 March 2004
R4	19 October 2004	1 November 2005	28 February 2005	2 March 2005

Mortality and grazing

Phytoplankton concentration decreases due to mortality and grazing. The rate of natural mortality (R_m) is taken as 0.1·day^{-1} at 10 °C (Spitz et al. 2003). Following Denman and Peña (2002), grazing is based on an annual fit to the observed dry weight of zooplankton. The dry weights used were collected as part of the STRATOGEM surveys using 236 μm mesh SCOR-type net (Sastri and Dower 2009). All tows were done during the day, so it was assumed that all zooplankton in the 100 m to surface tows could reach the euphotic zone to feed to ensure that most diel migrators were included. The 4 years of data were combined and a fit to the values (in μmol N·L^{-1}) was found:

$$\overline{Z} = Z_w + 0.525\exp\left[\frac{-(D-112)^2}{53.8^2}\right] + 0.152\exp\left[\frac{-(D-229)^2}{51.6^2}\right] + 0.0318\exp\left[\frac{-(D-316)^2}{14.6^2}\right] \quad (15)$$

where $\overline{Z}$ is the average zooplankton biomass over the model depth, Z_w is the winter concentration, and D is the day of the year. The weak fall zooplankton bloom has little impact on this study but is expected to be important in later studies considering summer and fall productivity.

Zooplankton are assumed to be able to choose their depth and thus mirror the phytoplankton concentration profile. Thus the zooplankton concentration as a function of depth is

$$Z = \overline{Z}\frac{P}{\overline{P}} \quad (16)$$

where $\overline{P}$ is the average phytoplankton concentration over the model depth.

Grazing is modeled with a hyperbolic growth function with a half-saturation constant κ_p = 1.0 μmol N·L^{-1} of phytoplankton based on observed winter concentrations of 0.5 μmol N·L^{-1} of phytoplankton (converted from total chlorophyll observations). Maximum ingestion Υ equals 0.6·day^{-1} at 10 °C (Cugier et al. 2005). The winter zooplankton concentration Z_w was the single tuned parameter. The fit gave a value of 0.073 μmol N·L^{-1}. The higher, tuned value of 0.168 μmol N·L^{-1} represents, in part, the unknown microzooplankton grazing pressure.

Temperature dependency

A temperature dependency of maximum growth rate, grazing, and mortality is implemented in the model by multiplying each by

$$\exp[\alpha_T(T - T_{ref})] \quad (17)$$

(Eppley 1972), where T_{ref} = 10 °C, α_T = 0.07·°C^{-1}, and T is modeled temperature. These functions are executed at all model depths.

An additional temperature effect is implemented only on the phytoplankton growth rate. *Thalassiosira nordenskioldii* is not observed to grow at temperatures of 18 °C and above (Durbin 1974). Thus the growth rate was multiplied by a linear decrease from one to zero as the temperature increases from 10 °C to 18 °C.

Sinking

Diatoms are negatively buoyant, particularly when nutrient-limited (Waite et al. 1992). Following Cugier et al. (2005), nutrient limitation is calculated as

$$f_N = \frac{N}{\kappa + N} \quad (18)$$

and then sinking speed is

$$w_s = W_1 f_N^{0.2} + W_2(1 - f_N^{0.2}) \quad (19)$$

where W_1 and W_2 are the sinking rates for nutrient-replete and nutrient-depleted diatoms, respectively.

Results

Physical model tuning and sensitivities

The physical model was run independently of the biological model over various time scales and compared with field data. The physical model was considered to be performing adequately when modeled physical profiles resembled observed physical profiles. To achieve this, internal mixing, vertical advection, and freshwater parameters were tuned, as described below. Profiles are generally well matched at depths below 30 m due to the bottom boundary conditions. For each run, the model was initialized with CTD data from either an October or a September cruise (Table 2) in the fall and run for one year and compared with later cruises, so that the model results could be compared with observations.

The value of the vertical advection velocity (adjusted through w_*) was set based on the analytic calculations and agrees with independent estimates in the Strait (Pawlowicz et al. 2007). It was not tuned. The amount of freshwater added to the Strait (F_w and σ_s in eq. 3) was tuned to give surface salinities that matched the empirical relationship (eq. 2*b*). The depth over which the freshwater was added (a_h in eq. 3) was tuned to give a good match between model and observed halocline depth. Most KPP parameters were set to the default values (Large et al. 1994) except the internal wave-mixing values (minimum mixing values) were in-

Fig. 5. Modeled daily-averaged mixing-layer depth (left axis, solid), daily-averaged wind magnitude cubed (right axis, shaded), and Fraser River flow (right axis, solid line) for 1 January to 1 October for each year: (*a*) 2002; (*b*) 2003; (*c*) 2004; and (*d*) 2005. Strong winds deepen the mixing-layer depth, whereas weak winds are associated with shallow mixing-layer depths. The Fraser River freshet coincides with a stable, shallow mixing-layer depth. Mixing-layer depths in January–February were deeper in 2002 (48.0 m) than in 2003 (3.11 m), 2004 (3.55 m), and 2005 (2.41 m), corresponding with stronger winds in 2002 (average wind speed cubed 340 $m^3 \cdot s^{-3}$) than in 2003 (240 $m^3 \cdot s^{-3}$), 2004 (220 $m^3 \cdot s^{-3}$), and 2005 (185 $m^3 \cdot s^{-3}$).

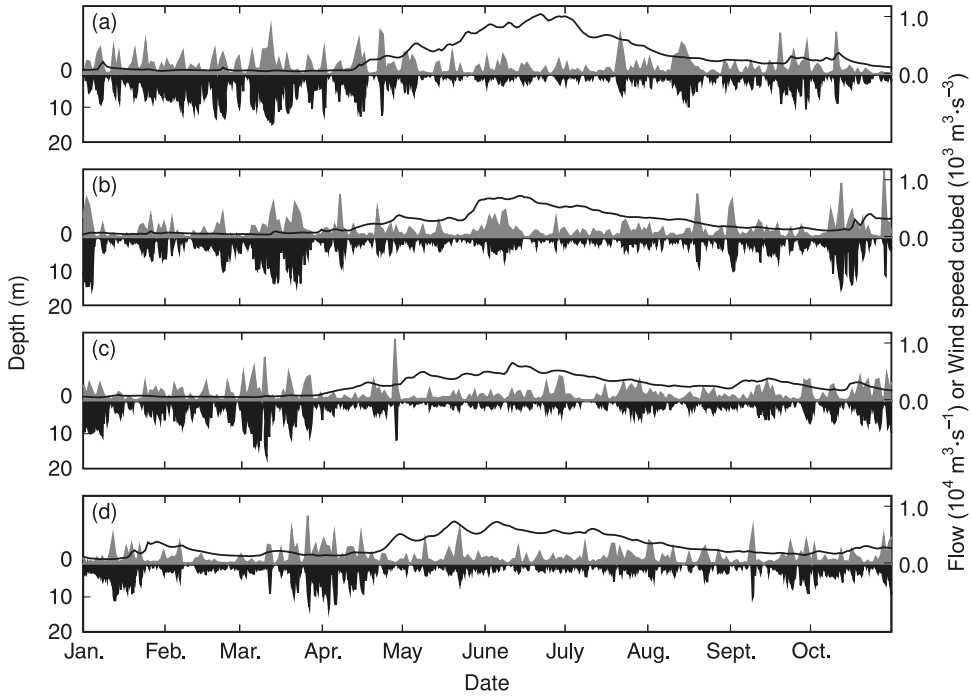

creased by 50% to reduce the strength of the model halocline, which was stronger than observed. This increase is consistent with the fact that the SoG has an active internal wave field due to strong tides over complicated topography to the north and south of the Strait (Gargett 1976). In addition, the shear diffusivity (eq. 28 in Large et al. (1994)) was slightly smoothed by adding 10% of the value above and below to 80% of the value calculated at a given depth; because the gradient Richardson number is a ratio of two differences, it is quite noisy, leading to sharp peaks and troughs in the shear diffusivity.

Physical model results

The KPP model calculates a mixing-layer depth based on a balance between kinetic energy and potential energy (Large et al. 1994). Wind is the sole mechanism through which kinetic energy is introduced into the model. The effect of wind mixing on the mixing-layer depth is expected to be proportional to the cube of wind speed (Fischer et al. 1979). A plot of KPP mixing-layer depth and wind speed cubed shows a clear relationship (Fig. 5). We see the deepest mixing-layer depths coinciding with strong winds, especially in the winter of 2002. A wind event in late August 2003 deepens the stable, shallow mixing layer from less than 1 m to greater than 10 m; the same type of event occurs in late April 2004.

The biggest source for potential energy input into the SoG is the freshwater inflow. The effect of the freshwater flux (which is proportional to the buoyancy flux) on the mixing layer is expected to be proportional to one over the flux (Fischer et al. 1979). In the model, this effect is particularly clear during the freshet when strong freshwater flux stratifies the water column and decreases the mixing-layer depth (Fig. 5). The mixing-layer depth is frequently deeper than 10 m in the fall and winter, but shallows to less than 5 m during the freshet. Wind events can disrupt the stratification produced by the layer of freshwater (late August 2003).

Model-calculated light above the surface compares well with data (Fig. 6) collected at the Halibut Bank Buoy (J. Gower, personal communication, 2005), which measures I_{PAR} at the surface. The correlation between modeled and observed surface irradiance is evidence that the estimation of light at 0 m done by the model — the cloud model and the estimation of how much of the total light is I_{PAR} — is predicting irradiance in the SoG reasonably successfully. Clouds are spatially variable over the Strait, with more clouds over land than water during certain times of the day and year and vice versa during other times. Clouds are also temporally variable. The fact that our model (based on observations at the airport) is agreeing, on average, with values from the Halibut Bank Buoy (Fig. 6) probably reflects the proximity of the airport to the Strait and the fact that prevailing winds bring air from the Strait over the airport.

The model predicts slightly warm temperature (Fig. 7*a*). Modeled and observed surface temperatures vary well together and are consistently within 1.5 °C of each other. Salinity is predicted well by the model, but less consistently than temperature (Fig. 7*a*). Modeled and observed surface salinity are, on average, within 2.1 of each other. The depth and strength of the thermocline and halocline are modeled

Fig. 6. Modeled (dotted lines) and observed (solid lines) surface irradiance for (*a*) 27 July – 5 August 2003, (*b*) 25 October – 16 November 2003; note that each panel is on a different scale: (*a*) during a relatively cloud-free period; (*b*) during cloudier conditions and showing that the model both over- and under-predicts irradiance.

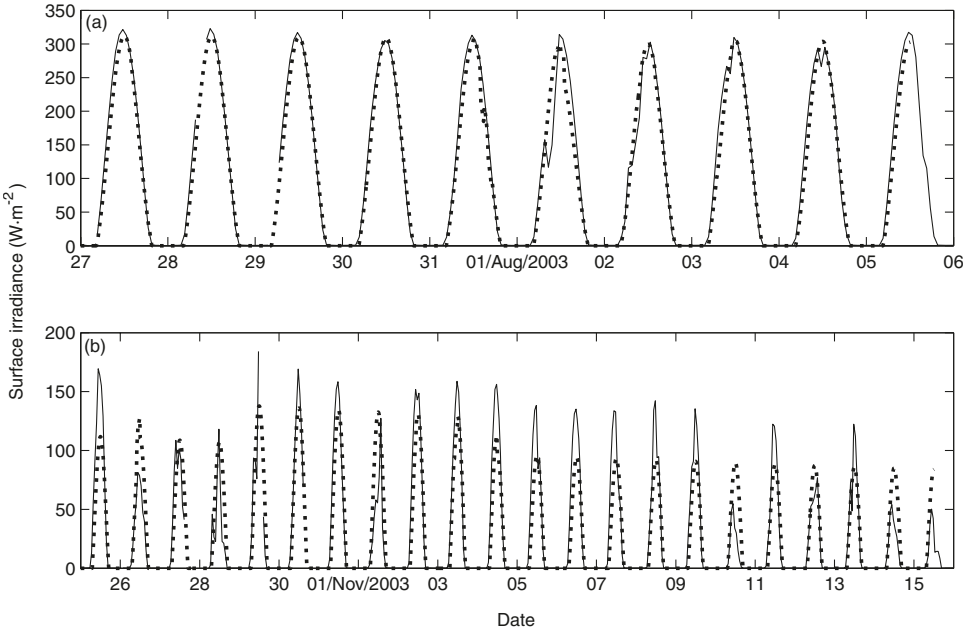

well in most cases. Irradiance profiles are generally well predicted by the model. Density is determined primarily by salinity (Fig. 7*b*). The model shows more evidence of a mixed layer than the data. As discussed above, the mixed layer is not as important as the mixing layer, and therefore more emphasis has been placed on matching the depth and strength of the halocline than the mixed-layer depth.

The model cannot include small-scale random variations that we observe in the SoG. In the example shown, the halocline is about 1 m too deep and the irradiance drops too slowly (Fig. 7). These errors are typical but not systematic; other examples show haloclines that are too shallow and irradiance that drops too fast.

Physical model performance

The manner in which the model responds to varied conditions in meteorological forcing such as high winds or increased freshwater input is a good indication of its success in modeling the physical system of the SoG. The physical model was forced with artificially high winds (low winds) and the mixing layer deepened (shallowed); tests with artificially high (low) Fraser River flow decreased (increased) surface salinity; and tests with forced clear (obscured) skies without changing air temperatures or humidity increased (decreased) water temperatures and light.

Biological model tuning and sensitivities

The SoG coupled biological–physical model was run in 13-month segments from September 2001 to November 2005; each run was initialized in September or October and run until November of the following year (Table 2). The biological model was tuned independently of the physical model. The only parameter tuned was the winter concentration of zooplankton, Z_w. For each of the four 13-month runs, surface modeled P was plotted and compared with both the high frequency ferry record of fluorescence and the discrete bottle-sampled chlorophyll (Fig. 8), and the surface-modeled N was compared with the discrete bottle-sampled nitrate (Fig. 9). The peak of the spring bloom was determined as the date of the maximum phytoplankton concentration within 4 days of the nitrate concentration going below 0.1 μmol·L^{-1}. One value for Z_w was found (Table 1) that produced optimal results for the timing of the spring bloom for the 4 years (Table 2).

The sensitivity of the modeled timing of the bloom to various parameters was determined (Table 3). The timing of the spring bloom was found to be relatively insensitive to the physical model parameters in KPP but strongly sensitive to biological parameters that affected the winter light-limited growth or the mortality. Increasing the optimal light level from 38.4 to 45 W·m^{-2} (17%) postpones the bloom an average of 26 days. Increasing the winter zooplankton concentration from 0.168 to 0.18 μmol N·L^{-1} (6%) postpones the bloom by an average of 6 days, and increasing the natural mortality from 0.1·day^{-1} to 0.11·day^{-1} (10%) postpones the bloom an average of 8 days.

The timing of the spring bloom is relatively insensitive to the initial profiles. Starting the model with a CTD–fluorescence–nitrate profile from a different year had no effect on the timing of the 2002, 2003, and 2004 spring blooms. However, the 2005 spring bloom changes by ±5 days. The 2005 bloom is sensitive to initial conditions because the winter phytoplankton concentrations remain higher than in the other years (Fig. 10) and, in particular, above the half-saturation constant for grazing. Thus, in 2005, the grazing term remains nearly linear and fall phytoplankton concentration information is transmitted through the winter.

Biological model results

The interannual variation of the arrival of the spring phy-

Fig. 7. Comparisons of model-predicted (thin lines) and observed (thick lines and points) data of physical and biological properties for 8 March 2005: (*a*) salinity (solid lines) and temperature (broken lines); (*b*) density (solid lines) and light (broken lines); (*c*) nitrate (solid line and solid circles) and chlorophyll fluorescence (broken lines, and solid diamonds are bottle-sampled chlorophyll $a > 20$ μm). Note that for nitrate there are only discrete samples and so no data line is shown.

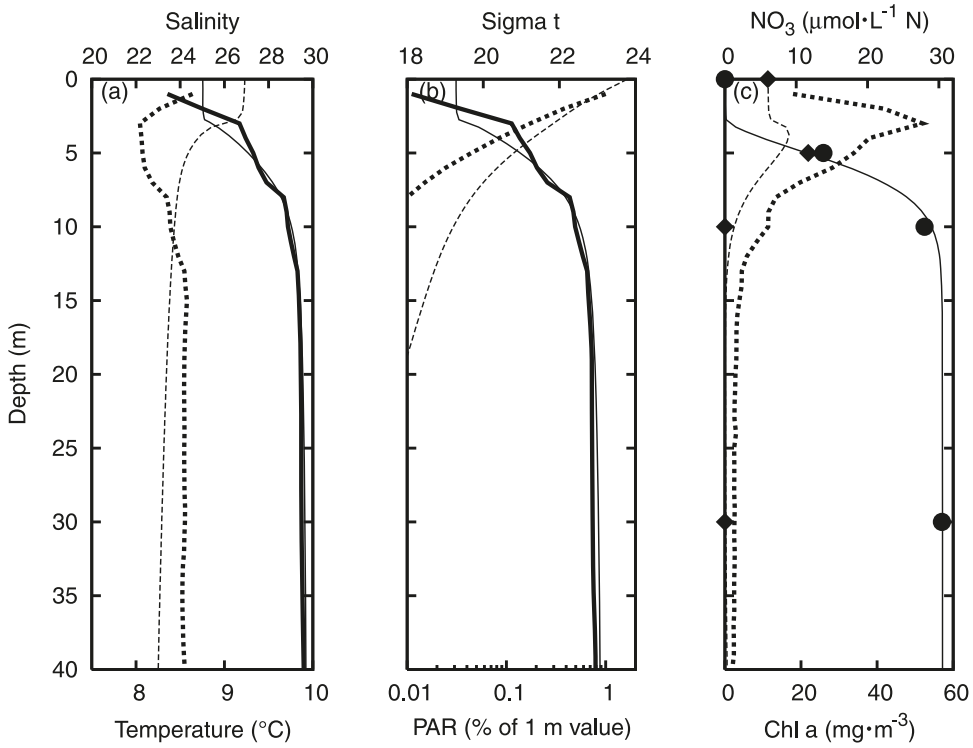

Fig. 8. Modeled surface phytoplankton (dark solid line), ferry fluorescence (shading), and bottle-sampled (>20 μm) chlorophyll (×s connected by broken line) for each year: (*a*) 2002; (*b*) 2003; (*c*) 2004; and (*d*) 2005. Ferry fluorescence absolute scale is poorly known and possibly changed between years. Vertical line marks 1 April each year.

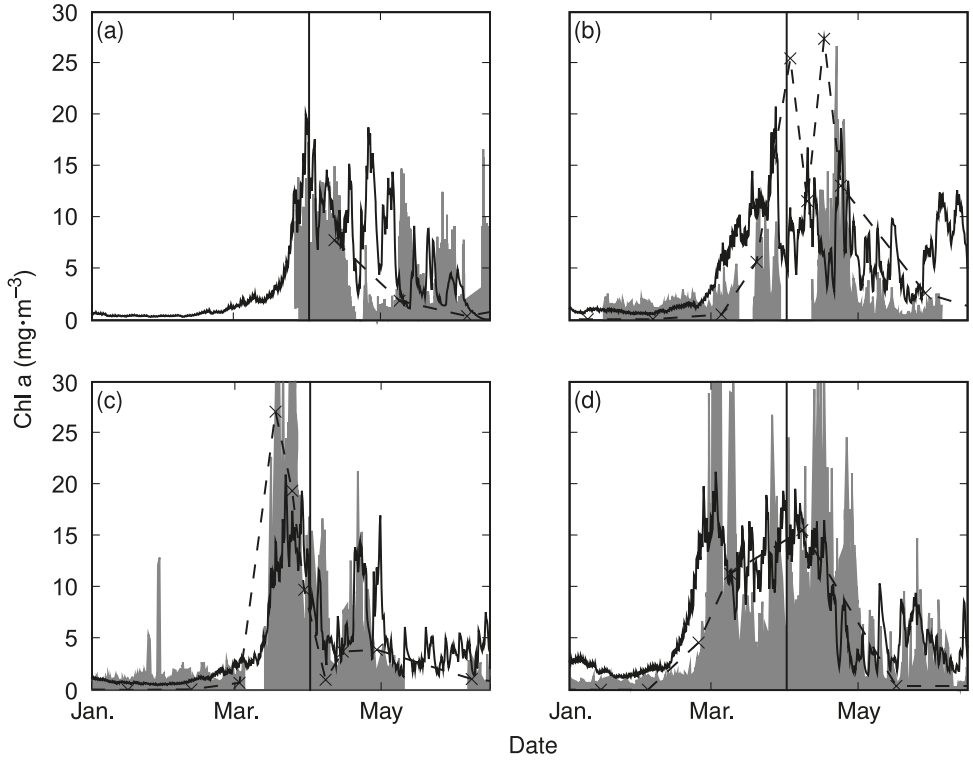

Fig. 9. Modeled surface nitrate (solid lines) and bottle-sampled nitrate (×s) for each year: (*a*) 2002; (*b*) 2003; (*c*) 2004; and (*d*) 2005.

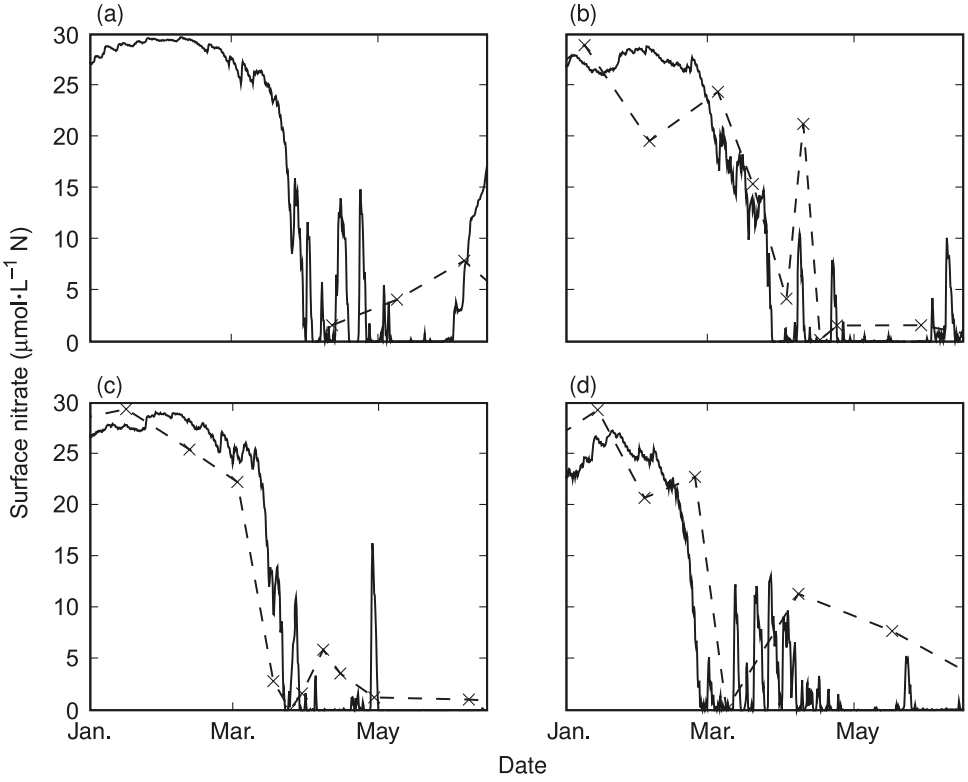

toplankton bloom is predicted successfully by the coupled biophysical model (Figs. 8 and 9). In each of the four sampled years, both the phytoplankton bloom arrival, peak, and decline and the nitrate depletion occur within 3 days of that observed in the field. Nitrate levels throughout the winter increase to levels that are seen in the field, whereas *P* decreases to low levels during the light-limited winter months.

Another measure of the success of the model is the comparison of the modeled biological parameters to the CTD observations (Fig. 7*c*). The nitrate is generally well matched at the surface and through the mixing-layer depth, and the slope of depletion with depth is well predicted (Fig. 7*c*). The model often underpredicts phytoplankton compared with observed fluorescence (CTD) because fluorescence represents all the phytoplankton in the water column and the model only includes diatoms. A better comparison tool is bottle-sampled chlorophyll in the >20 μm size class. During the spring bloom, the >20 μm size class represents 40%–60% of the total measured chlorophyll, which would account for most of the difference seen between the modelled and measured fluorscence chlorophyll values. However, even compared with the bottle-sampled chlorophyll, the magnitude of the bloom is consistently underpredicted by the model (Fig. 8). We suggest that this is due to the absence of the ammonium regeneration loop that provides an alternate food source for phytoplankton and perhaps to using too low a chlorophyll-to-nitrogen ratio for the phytoplankton.

Discussion

Interannual differences in the Strait of Georgia

Variations within the physical and biological environments over the four sampled years were significant. Wind at Sandheads was strongest for the January through March period in 2002 (mean wind speed was 5.62 m·s^{-1}), followed closely by 2003 (5.04 m·s^{-1}) and 2004 (5.07 m·s^{-1}), and was significantly weaker in 2005 (3.24 m·s^{-1}); the 30-year mean for this period is 5.16 m·s^{-1} (Environment Canada 2002). The Fraser River freshet was greater than the climatological mean by more than 3×10^3 m^3·s^{-1} in 2002, and early 2005 flow was four times greater than mean winter flow (Environment Canada 2006); flow in 2003 and 2004 was average. In January 2005, total precipitation was 249.6 mm compared with a 30-year mean of 153.6 mm; February total precipitation was 45.8 mm compared with a 30-year mean of 123.1 mm (Environment Canada 2002). February 2005 had 139.9 h of bright sunshine, a 30-year maximum and far greater than the 30-year mean of 84.6 h (Environment Canada 2002). The arrival of the spring bloom also varied greatly over the sampling period, peaking earliest in 2005 (February 28) and latest in 2002 (April 1).

What factors control the spring bloom?

Before the spring bloom, strong wind speed cubed decreases the surface chlorophyll concentration and indeed the depth-averaged chlorophyll (not shown). As winds increase the mixing-layer depth, the phytoplankton are mixed to depths without sufficient light to grow. Almost every decrease in the time series is correlated with strong wind, and it appears that blooms are significantly delayed after winters with many strong storms. After the spring bloom, strong winds have the opposite effect; they mix nutrients into the nutrient-exhausted surface layer and increase the chlorophyll concentration.

Table 3. Sensitivity of the spring bloom date with regards to various model parameters.

Parameter	Standard value	Substituted value	Average bloom change (days)
Background momentum (scalar) mixing	1.5×10^{-4} (10^{-5}) $m^2 \cdot s^{-1}$	1.0×10^{-4} (10^{-5}) $m^2 \cdot s^{-1}$	+2.5
	1.5×10^{-4} (10^{-5}) $m^2 \cdot s^{-1}$	2.0×10^{-4} (10^{-5}) $m^2 \cdot s^{-1}$	–1
Sheer smoothing (fraction above and below)	0.1	0.15	–1.5
	0.1	0.05	+0.75
Mesozooplankton, winter concentration	0.168 μmol $N \cdot L^{-1}$	0.15 μmol $N \cdot L^{-1}$	–14
	0.168 μmol $N \cdot L^{-1}$	0.18 μmol $N \cdot L^{-1}$	+6
Mesozooplankton, summer concentration (multiplied by)	1.0	0.9	–8
	1.0	1.1	+5
Mesozooplankton, ingestion	$0.6 \cdot day^{-1}$	$0.59 \cdot day^{-1}$	–3
	$0.6 \cdot day^{-1}$	$0.61 \cdot day^{-1}$	+1.25
Mesozooplankton, half-saturation	1.0 μmol $N \cdot L^{-1}$	0.75 μmol $N \cdot L^{-1}$	0
	1.0 μmol $N \cdot L^{-1}$	1.5 μmol $N \cdot L^{-1}$	–22
Diatom, I_{opt}	38.4 $W \cdot m^{-2}$	35.0 $W \cdot m^{-2}$	–20
	38.4 $W \cdot m^{-2}$	45.0 $W \cdot m^{-2}$	+26
Diatom, maximum temperature	18 °C	15 °C	+45
	18 °C	22 °C	0
Diatom, half-saturation nitrate	1.0 μmol $N \cdot L^{-1}$	0.5 μmol $N \cdot L^{-1}$	0
	1.0 μmol $N \cdot L^{-1}$	1.5 μmol $N \cdot L^{-1}$	–0.25
Diatom, natural mortality	$0.1 \cdot day^{-1}$	$0.086 \cdot day^{-1}$	–17
	$0.1 \cdot day^{-1}$	$0.11 \cdot day^{-1}$	+8

Note: The date of the bloom is most sensitive to parameters directly affecting the light-limited winter growth (optimal light level, maximum temperature for growth (when its low)) and those directly affecting loss terms (natural mortality rate and mesozooplankton concentration, ingestion rate, and half-saturation point (when its high)).

Fig. 10. Daily-averaged wind speed cubed (left axis, shading) and modeled surface chlorophyll (right axis, solid line) for all four years: (*a*) 2002; (*b*) 2003; (*c*) 2004; and (*d*) 2005. Note that chlorophyll is on a log scale. Winds are strongest in 2002 (*a*) and weakest in 2005 (*d*); the bloom is latest in 2002 (*a*) and earliest in 2005 (*d*). (Maximum daily-averaged wind speed cubed reaches 5082 $m^3 \cdot s^{-3}$ in December 2001.)

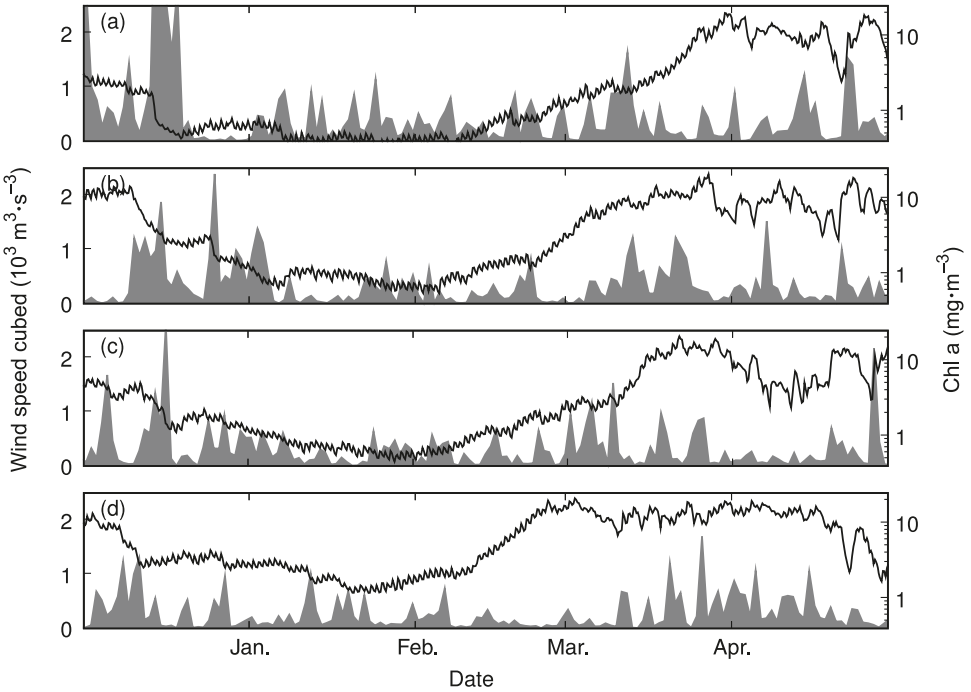

To quantify the effect of different physical forcings on the arrival time of the spring bloom, a series of 74 tests was done using various data sets. In each test, one variable (clouds, Fraser River flow, or wind) was replaced with either artificial data or data from another time period; all other variables remained constant. For example, the run "R1c00" (Table 4) was initialized in September 2001 and run until November 2002 with all data from 2001–2002 except the

Table 4. List of run tests that were done to determine the impact of the various forcing factors.

Code	Base years	Forcing varied	Value of changed forcing
R*wR1	R2, R3, R4	Wind	R1 wind
R*wR2	R1, R3, R4	Wind	R2 wind
R*wR3	R1, R2, R4	Wind	R3 wind
R*wR4	R1, R2, R3	Wind	R4 wind
R*w050	R1, R2, R3, R4	Wind	0.5*wind
R*w080	R1, R2, R3, R4	Wind	0.8*wind
R*w125	R1, R2, R3, R4	Wind	1.25*wind
R*w200	R1, R2, R3, R4	Wind	2*wind
R*cR1	R2, R3, R4	Clouds	R1 clouds
R*cR2	R1, R3, R4	Clouds	R2 clouds
R*cR3	R1, R2, R4	Clouds	R3 clouds
R*cR4	R1, R2, R3	Clouds	R4 clouds
R*c00	R1, R2, R3, R4	Clouds	None
R*c035	R1, R2, R3, R4	Clouds	0.35
R*c10	R1, R2, R3, R4	Clouds	1.0
R*fR1	R2, R3, R4	Freshwater	R1 freshwater
R*fR2	R1, R3, R4	Freshwater	R2 freshwater
R*fR3	R1, R2, R4	Freshwater	R3 freshwater
R*fR4	R1, R2, R3	Freshwater	R4 freshwater
R*f050	R1, R2, R3, R4	Freshwater	0.5*freshwater
R*f200	R1, R2, R3, R4	Freshwater	2*freshwater
R3fR4×2	R3	Freshwater	2*R4 freshwater
R4fR3/2	R4	Freshwater	0.5*R3 freshwater

Note: List of the base runs is given in Table 2. The asterisk (*) in the code is replaced by the number of the base run in column 2.

cloud data, which were set to 0 for the entire run. "R1cR2" was run for the same period, but clouds were replaced with clouds from 2003; this less extreme type of data set produced more realistic results than the data sets that were constant values.

Wind

The bloom arrival times varied significantly with different wind data sets (Fig. 11*a*) such that weak winds cause the bloom to arrive earlier than strong winds, which delay the bloom. Low wind mixing in the SoG provides the stratification necessary for a bloom to develop, whereas strong wind mixing prevents stratification. For realistic average wind speeds (>5 $m \cdot s^{-1}$ and <9 $m \cdot s^{-1}$), there is a linear relationship between wind strength and bloom arrival time (Fig. 11*a*). At both higher and lower wind speeds, the bloom date is a weaker function of wind speed. The linear relationship follows

$$\text{Year day of bloom peak} = 11.3\ \text{days} \cdot \text{m}^{-1} \cdot \text{s} \cdot \langle W^3 \rangle^{1/3} + \text{Dec. 30} \quad (20)$$

where $\langle W^3 \rangle^{1/3}$ is the cubed root of the December to February averaged wind speed cubed. The root mean square of the residuals is 7.3 days. The fit is based on the model results (open symbols in Fig. 11); the four observations (solid symbols in Fig. 11) are within the scatter of model results and are consistent with the same slope. Runs "R1wR4", "R2wR4", and "R3wR4" were forced with 2005 wind and had bloom peak dates of more than 2 weeks earlier than "R1", "R2", and "R3". The half-wind scenarios (R*w050) caused the bloom to arrive earlier than for any other scenario in Table 4.

The historical record (1968–2006) shows variations of 6.0–8.9 $m \cdot s^{-1}$ for the cubed-root December to February averaged cubed wind speed. This would correspond to a variation in spring bloom timing of 33 days due to the wind alone.

Cloud cover

Variations in cloud cover have a weaker effect on the timing of the spring bloom (Fig. 11*b*). When the model is tested with clouds from different years, the bloom peak dates are all within 10 days of each other. However, including no clouds and full cloud cover, a strong trend is evident with more clouds delaying the bloom. The curve is less steep than that for wind, suggesting that wind controls the timing of the bloom with light having a secondary effect.

The historical record (1968–2006) shows variations of 0.60 to 0.85 for the December to February averaged cloud fraction. Given the slope implied here (about 60 days), the historical variation due to cloud fraction would be about 15 days or half that due to the wind speed.

Fraser River flow

Variations in Fraser River flow do not cause a consistent pattern in bloom arrival time (Fig. 11*c*). There is a tendency for high freshwater flow to move the bloom earlier; stronger stratification leads to both a shallower mixing layer and weaker estuarine advection. Also, following any particular run, at low freshwater flow, there is also a tendency to move the bloom earlier; this is probably the response to weaker advection that occurs if the freshwater flow, and thus the estuarine circulation, is weaker. Note that the freshwater flux has a much more direct impact on the stratifica-

Fig. 11. Results of model testing gave different bloom arrival dates for different wind (cubed root of the average December to February wind speed cubed), cloud patterns (average cloud fraction from December to January), and freshwater flow (average effective total freshwater (eq. 2*a*) from December to January). Solid symbols represent actual peak bloom. Open squares, circles, upward triangles, and downward triangles represent R1, R2, R3, and R4 runs, respectively. As wind magnitude increases, the arrival date of the bloom is later; this relationship is strong. Cloud fraction plays a secondary role in the timing of the bloom. There is no clear relationship between date of bloom peak and river flow.

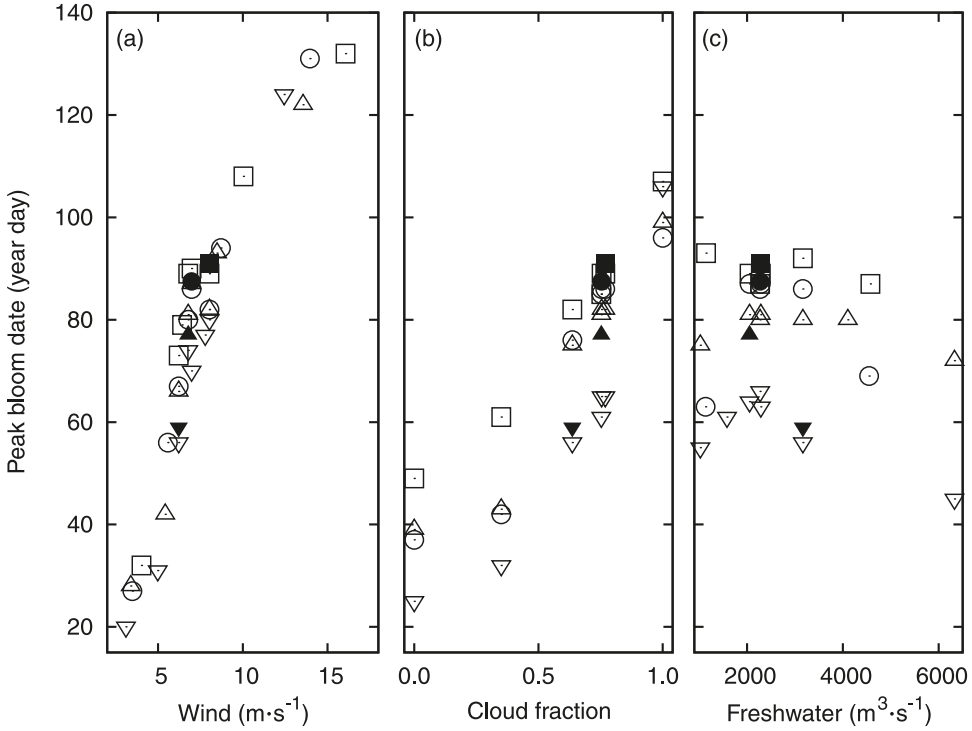

tion, as can be seen by the small mixing-layer depth during the freshet, than it does on the spring bloom timing. For winter–spring phytoplankton in the SoG, the estuarine advection term (a loss term) is as important as the freshwater-induced reduction in mixing-layer depth (which impacts the light levels for the phytoplankton and thus the growth term).

Empirical fit

A linear fit on the cubed root of the average wind speed cubed is a good representation of the bloom date for the runs with wind manipulated. Here we estimate an empirical fit for all the runs in Table 4. The shape of the bloom peak date versus wind strength (Fig. 11*a*) for all winds suggests a decreasing slope at high winds and low winds $A_1\omega^2/(A_2^2+\omega^2)$, where $\omega = \langle W^3\rangle^{1/3}$ is the cubed root of the mean cubed wind speed and A_1 and A_2 are constants. The bloom date increases with cloud fraction $A_3c_f^2$, where A_3 is another constant and c_f is the cloud fraction. In both cases, the parameters squared gave a better fit than without squaring. Following the structure of the estuarine vertical advection with total freshwater flow, we implement the effect of the freshwater with $A_4(Q_T/\overline{Q})\exp(-Q_T/\overline{Q})$. This gives

$$\text{Year day of bloom peak} = \frac{A_1\omega^2}{A_2^2+\omega^2} + A_3c_f^2 + A_4(Q_T/\overline{Q})\exp(-Q_T/\overline{Q}) + A_5 \quad (21)$$

where A_5 is another constant. A multiple least squares fit gives

Fig. 12. Comparison of bloom arrival date predicted by eq. 21 with dates predicted from model testing with different cloud, wind, and Fraser River scenarios. Thin lines are ±7 days; plus signs (+) are model results, and solid circles are the observations.

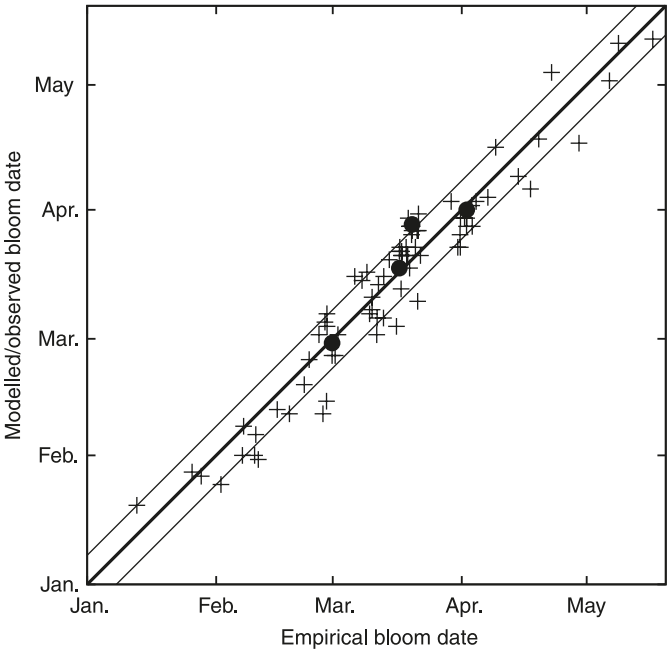

$$A_1 = 167 \text{ days},\ A_2 = 6.85 \text{ m} \cdot \text{s}^{-1},\ A_3 = 66.0 \text{ days},\ A_4 = 34.7 \text{ days},\ A_5 = -54.8 \text{ days} \quad (22)$$

with a root mean square of the residuals of 6.6 days (Fig. 12). The empirical fit implies a variation of peak bloom date of 21 days due to the winds, 11 days due to the clouds, and 1.5 days due to the freshwater, over the observed 2002–2005 range of these parameters.

Model limitations

Each parametrization in the physical model for the SoG has inherent limitations. The freshwater flux parametrization was extensive and based on innovative methods and a wide range of data. The surface salinity in the model is calculated based on a regression of daily flow estimates and matched to the 15 min model time step in a smoothing procedure; freshwater flux calculations depend on this value. All these steps introduce the possibility of error and inaccuracy, but well-modeled salinity implies that error introduced by these parametrizations is small.

Uncertainty in the calculation for I_{PAR} is derived from the multivariable nature of the attenuation coefficient (eq. 8). One of these variables is calculated by the model and thus depends on another set of variables and equations and associated uncertainty. The total light scheme depends on eqs. 8, 9*a*, and 9*b*), of which the latter two are based on data from Jerlov (1976).

A diverse biological community inhabits the SoG, including many different sizes and species of both phytoplankton and zooplankton, and a complex regeneration cycle (R. Pawlowicz, A.R. Sastri, S.E. Allen, D. Cassis, O. Riche, M. Halverson, R. El-Sabaawi, and J.F. Dower, unpublished data). Although the biological model includes only one phytoplankton group and one nutrient source, results show that these parameters, arguably the most important in terms of spring bloom development, are adequate to predict interannual variability in the timing of the spring bloom. The growth rate was chosen to lie between published *Thalassiosira* spp. growth rates. To look at the sensitivity of that choice, we also considered growth rates of 1.8·day^{-1}and 2.6·day^{-1} (24 h at 10 °C). For each growth rate, we re-tuned the model by changing the winter zooplankton biomass (to 0.056 μmol N·L^{-1} and 0.287 μmol N·L^{-1}, respectively) and re-ran a subset of the test runs. Then we re-fit the empirical relation between the winds, cloud fraction, freshwater, and the predicted bloom date. For cubed-root of average wind speeds cubed below 8 m·s^{-1}, the results were within 7 days of the base case. For greater wind speeds, lower growth rates predict later blooms than do higher growth rates. The changes in growth rate chosen were large, about ±20%. Even with these changes, only the magnitude of the dependence on the wind and cloud fraction change.

As temperature in the SoG is not important to the stratification, the systematic slightly warm temperatures in the model mainly impact the results through the temperature dependence on growth, mortality, and grazing. Thus the temperature error has an equivalent effect as a change in the biological parameters much smaller than the change in growth rate discussed above.

If we wish to use the model in a predictive mode, we must be conscious of the large sensitivity of the model (and probably the real spring bloom) to the biological parameters and whether these values may change. The largest possible changes would come either from a change in phytoplankton community and thus in growth rate and optimal light levels or from a change in number or species of overwintering zooplankton. If significant shifts occur in either of these communities, the model will not be able to predict the shift in the timing of spring bloom.

Thus the model is not sensitive to the choice of parameters if we re-tune it. The result that the timing of the spring bloom is primarily dependent on the wind speed and secondarily on the cloud fraction is robust to large changes in the parameters. However, shifts in either growth rate or loss parameters that are not balanced will cause "biological" shifts in the timing of the spring bloom that are not dependent on the physical forcings.

Comparison with other results

Previous research on bloom dynamics in the SoG suggests that a stratified water column is necessary for a bloom to occur and that this stratification is achieved by freshwater input and destroyed by winds greater than 4 m·s^{-1} (Yin et al. 1997*b*). Yin et al. (1997*b*) further assert that the bloom will not fully develop until the freshwater discharge is strong enough to overcome wind and tidal mixing and that the bloom arrival is dependent on the freshet arrival (Yin et al. 1996). This theory is not supported by the results presented here, which show that the freshwater flux has no consistent effect on the bloom arrival time (Fig. 11*b*). The relationship between wind and bloom arrival time discussed here agrees with Yin's claim that wind can delay the bloom (Yin et al. 1997*b*). These previous results were based on cruises during 1991, which had a winter (December–February) with similar winds and clouds to 2003 or 2004 but high freshwater flux similar to 2005.

A coupled physical and biological two-layer box model found that plankton populations were insensitive to interannual changes in estuarine circulation caused by variability in Fraser River discharge (Li et al. 2000), a result that agrees with our research. Li et al. (2000) did not explicitly test the model's sensitivity to wind or changes in light availability but suggested that variations in biological parameters could cause interannual timing variations. We would propose that this variability is primarily due to variations in light intensity due to wind mixing or clouds that were not explicitly modeled in Li's study.

A number of models aiming to investigate dependence of the interannual variability in the timing of the spring bloom on the physical environment exist, with varying degrees of similarity to this study. These models are often 1D physical models, whereas biological models range in their complexity. Unlike Prince William Sound and the Bering Sea, the SoG stratification is dominated by salinity variations due to strong freshwater runoff. However, as in Prince William Sound (Eslinger et al. 2001) and the Bering Sea (Jin et al. 2006), we have shown that in the SoG, the dominant influence on the timing of the spring bloom is interannual variations in the wind. On the other hand, a study in an estuary off the UK coast using linear and stepwise regression analyses between chlorophyll *a* concentration and each of mean water column I_{PAR}, river flow, tidal range, and wind speed

found no clear relationship between wind speed and the timing of the spring bloom (Iriarte and Purdie 2004). The authors concluded that the main factor controlling the timing of the bloom in this location is irradiance. Similarly, results from a 1D NPZD model coupled to the finite volume coastal ocean model (FVCOM) showed that over the shallow, well-mixed region of George's Bank, the timing of the bloom depends on light intensity and attenuation (Ji et al. 2006). These results are not surprising as mixing is dominated by tides not winds for both these regions.

Implications

The results for the SoG on the timing of the spring bloom have implications for other regions. First, in regions with strong buoyancy fluxes, the mixing layer may exceed the depth of the mixed layer and thus blooms may not occur even if the Sverdrup critical depth exceeds the mixed-layer depth. Second, in estuaries or other regions with estuarine circulation, the freshwater flux has two opposing effects on the timing of the spring bloom. Increased freshwater flux increases the stratification and thus increases the phytoplankton growth rate but increased freshwater flux also increases estuarine circulation and thus increases the phytoplankton loss rate. Third, considering the results from other regions described above, in regions where wind mixing dominates over tidal mixing, interannual variations in the wind speed will have a significant effect on the interannual variation of the timing of the spring bloom.

The major result of this study is that the spring bloom in the Strait of Georgia is controlled primarily by the wind, with high winds causing a late bloom and weak winds causing an early bloom, and secondarily by the amount of cloud. Edwards and Richardson (2004) assert that changes in the synchrony of timing between primary, secondary, and tertiary production affects marine trophodynamics, including commercially important fish stocks. Mean spring wind speed has decreased over the last 35 years in the Strait of Georgia, but wind forecasts for this region range from rising temperatures leading to reduced global wind fields to rising temperatures leading to increased local wind (Boesch et al. 2000). Although the wind forecast is unclear, this study implies that as wind patterns change, we can expect a change in spring bloom timing, with subsequent effects carrying through to the upper trophic levels.

Acknowledgments

John Gower of Fisheries and Oceans Canada provided the 2001–2005 irradiance at Halibut Bank Buoy data and Rick Ketler of UBC Department of Agroecology provided the 2001–2005 solar radiation data. Kira Jang did the sensitivity studies. Doug Latornell made the model more efficient and prepared a number of the figures. The excellent data set used in this study would not have been collected without the efforts of the crew of the CGS *Siyay* and the many scientists who participated in the cruises. The ferry data were collected from BC Ferries, primarily the *Queen of New Westminister*. The manuscript was significantly improved based on comments from three anonymous reviewers. The second author would like to thank Alain Ménesguen for his useful suggestions and hospitality while she was on sabbatical at IFREMER.

References

Batchelor, G.K. 1967. An introduction to fluid dynamics. Cambridge University Press, Cambridge, UK.

Beamish, R.J., Benson, A.J., Sweeting, R.M., and Neville, C.M. 2004. Regimes and the history of the major fisheries off Canada's west coast. Prog. Oceanogr. **60**(2–4): 355–385. doi:10.1016/j.pocean.2004.02.009.

Boesch, D.F., Field, J.C., and Scavia, D. (*Editors*). 2000. The potential consequences of climate variability and change on coastal areas and marine resources. NOAA Center for Sponsored Coastal Ocean Research, Silver Spring, Maryland. Decision Analysis Series No. 21.

Campin, J.M., Marshall, J., and Ferreira, D. 2008. Sea ice–ocean coupling using a rescaled vertical coordinate z^*. Ocean Model. **24**(1–2): 1–14. doi:10.1016/j.ocemod.2008.05.005.

Chassignet, E.P., Smith, L.T., Halliwell, G.R., and Bleck, R. 2003. North Atlantic simulation with the HYbrid Coordinate Ocean Model (HYCOM): impact of the vertical coordinate choice, reference density, and thermobaricity. J. Phys. Oceanogr. **33**(12): 2504–2526. doi:10.1175/1520-0485(2003)033<2504:NASWTH>2.0.CO;2.

Cugier, P., Ménesguen, A., and Guillaud, J.F. 2005. Three-dimensional (3D) ecological modelling of the Bay of Seine (English Channel, France). J. Sea Res. **54**(1): 104–124. doi:10.1016/j.seares.2005.02.009.

Denman, K.L., and Peña, M.A. 2002. The response of two coupled one-dimensional mixed layer/planktonic ecosystem models to climate change in the NE subarctic Pacific Ocean. Deep Sea Res. Part II Top. Stud. Oceanogr. **49**(24-25): 5739–5757. doi:10.1016/S0967-0645(02)00212-6.

Dickson, M.-L., and Wheeler, P.A. 1995. Nitrate uptake rates in a coastal upwelling regime: a comparison of PN-specific, absolute, and chl *a*-specific rates. Limnol. Oceanogr. **40**: 533–543.

Dobson, F.W., and Smith, S.D. 1988. Bulk models of solar radiation at sea. Q. J. R. Meteorol. Soc. **114**: 165–182.

Durbin, E.G. 1974. Studies on the autecology of the marine diatom *Thalassiosira nordenskioldii* cleve, 1. The influence of day-length, light intensity, and temperature on growth. J. Phycol. **10**: 220–225.

Durski, S.M., Glenn, S.M., and Haidvogel, D.B. 2004. Vertical mixing schemes in the coastal ocean: comparison of the level 2.5 Mellor–Yamada scheme with an enhanced version of the K profile parameterization. J. Geophys. Res. **109**(C1): C01015. doi:10.1029/2002JC001702.

Edwards, M., and Richardson, A.J. 2004. Impact of climate change on marine pelagic phenology and trophic mismatch. Nature (London), **430**(7002): 881–884. doi:10.1038/nature02808. PMID:15318219.

El-Sabaawi, R., Dower, J.F., Kainz, M., and Mazumder, A. 2009. Interannual variability in fatty acid composition of the copepod *Neocalanus plumchrus* in the Strait of Georgia, British Columbia. Mar. Ecol. Prog. Ser. **382**: 151–161. doi:10.3354/meps07915.

Environment Canada. 2002. Climate database [online]. Available at http://www.climate.weatheroffice.ec.gc.ca/climateData/canada_e.html.

Environment Canada. 2006. Hydrometric data [online]. Available at http://www.wsc.ec.gc.ca/.

Eppley, R.W. 1972. Temperature and phytoplankton growth in the sea. Fish. Bull. (Washington, D.C.), **70**(4): 1063–1081.

Erga, S.R., and Heimdal, B.R. 1984. Ecological studies on the phytoplankton of Korsfjorden, western Norway. The dynamics of a spring bloom seen in relation to hydrographical conditions and light regime. J. Plankton Res. **6**(1): 67–90. doi:10.1093/plankt/6.1.67.

Eslinger, D.L., Cooney, R.T., McRoy, C.P., Ward, A., Kline, T.C., Jr., Simpson, E.P., Wang, J., and Allen, J.R. 2001. Plankton dynamics: observed and modelled response to physical conditions in Prince William Sound, Alaska. Fish. Oceanogr. **10**(Suppl. 1): 81–96. doi:10.1046/j.1054-6006.2001.00036.x.

Falkowski, P.G. 1975. Nitrate uptake in marine phytoplankton: comparison of half-saturation constants from seven species. Limnol. Oceanogr. **20**(3): 412–417.

Fasham, M.J.R., Ducklow, H.W., and McKelvie, S.M. 1990. A nitrogen-based model of plankton dynamics in the oceanic mixed layer. J. Mar. Res. **48**: 591–639.

Fischer, H.B., List, E.J., Koh, R.C.Y., Imberger, J., and Brooks, N.H. 1979. Mixing in inland and coastal waters. Academic Press, San Diego, California.

Friedrichs, M.A.M., Hood, R.R., and Wiggert, J.D. 2006. Ecosystem model complexity versus physical forcing: quantification of their relative impact with assimilated Arabian Sea data. Deep Sea Res. Part II Top. Stud. Oceanogr. **53**(5-7): 576–600. doi:10.1016/j.dsr2.2006.01.026.

Gargett, A.E. 1976. Generation of internal waves in the Strait of Georgia, British Columbia. Deep-Sea Res. **23**: 17–20.

Harrison, P.J., Fulton, J.D., Taylor, F.J.R., and Parsons, T.R. 1983. Review of the biological oceanography of the Strait of Georgia: pelagic environment. Can. J. Fish. Aquat. Sci. **40**(7): 1064–1094. doi:10.1139/f83-129.

Herlinveaux, R.H., and Tully, J.P. 1961. Some oceanographic features of the Juan de Fuca Strait. J. Fish. Res. Board Can. **18**: 1027–1071.

Hetland, R.D., and MacDonald, D.G. 2008. Spreading in the near-field Merrimack River plume. Ocean Model. **21**(1–2): 12–21. doi:10.1016/j.ocemod.2007.11.001.

Hitchcock, G.L. 1980. Influence of temperature on the growth rate of *Skeletonema costatum* in response to variations in daily light intensity. Mar. Biol. (Berl.), **57**(4): 261–269. doi:10.1007/BF00387569.

Hobson, L.A., and McQuoid, M.R. 1997. Temporal variations among planktonic diatom assemblages in a turbulent environment of the southern Strait of Georgia, British Columbia, Canada. Mar. Ecol. Prog. Ser. **150**: 263–274. doi:10.3354/meps150263.

Huisman, J., van Oostveen, P., and Weissing, F.J. 1999. Critical depth and critical turbulence: two different mechanisms for the development of phytoplankton blooms. Limnol. Oceanogr. **44**: 1781–1787.

Iriarte, A., and Purdie, D.A. 2004. Factors controlling the timing of major spring bloom events in an UK south coast estuary. Estuar. Coast. Shelf Sci. **61**(4): 679–690. doi:10.1016/j.ecss.2004.08.002.

Jeffery, N. 2002. Modelling a phytoplankton dichotomy in the eastern subarctic Pacific: impact of atmospheric variability, iron surface flux, and life cycle dynamics of the calanoid copepods, *Neocalanus* spp. Ph.D. thesis, University of British Columbia, Vancouver, British Columbia.

Jerlov, N.G. 1976. Marine optics. Vol. 14. Elsevier Oceanography Series, Elsevier Scientific Publishing Company, New York.

Ji, R.B., Chen, C.S., Franks, P.J.S., Townsend, D.W., Durbin, E.G., Beardsley, R.C., Lough, R.G., and Houghton, R.W. 2006. Spring phytoplankton bloom and associated lower trophic level food web dynamics on Georges Bank: 1-D and 2-D model studies. Deep Sea Res. Part II Top. Stud. Oceanogr. **53**(23-24): 2656–2683. doi:10.1016/j.dsr2.2006.08.008.

Jin, Z., Charlock, T.P., Smith, W.L., and Rutledge, K. 2004. A parameterization of ocean surface albedo. Geophys. Res. Lett. **31**(22): L22301. doi:10.1029/2004GL021180.

Jin, M., Deal, C.J., Wang, J., Tanaka, N., and Ikeda, M. 2006. Vertical mixing effects on the phytoplankton bloom in the southeastern Bering Sea mid-shelf. J. Geophys. Res. **111**(C3): C03002. doi:10.1029/2005JC002994.

Kettle, A.J. 2005. Comparison of the nonlocal transport characteristics of a series of one-dimensional oceanic boundary layer models. Ocean Model. **8**(4): 301–336. doi:10.1016/j.ocemod.2004.01.002.

Kobari, T., and Ikeda, T. 2001. Ontogenetic vertical migration and life cycle of *Neocalanus plumchrus* (Crustacea: Copepoda) in the Oyashio Region, with notes on regional variations in body sizes. J. Plankton Res. **23**(3): 287–302. doi:10.1093/plankt/23.3.287.

Large, W.G., and Pond, S. 1982. Sensible and latent heat flux measurements over the ocean. J. Phys. Oceanogr. **12**(5): 464–482. doi:10.1175/1520-0485(1982)012<0464:SALHFM>2.0.CO;2.

Large, W.G., McWilliams, J.C., and Doney, S.C. 1994. Oceanic vertical mixing: a review and a model with a nonlocal boundary layer parameterization. Rev. Geophys. **32**(4): 363–403. doi:10.1029/94RG01872.

Li, M., Gargett, A., and Denman, K. 2000. What determines seasonal and interannual variability of phytoplankton and zooplankton in strongly estuarine systems? Application to the semi-enclosed estuary of Strait of Georgia and Juan de Fuca Strait. Estuar. Coast. Shelf Sci. **50**: 467–488. doi:10.1006/ecss.2000.0593.

MacDonald, D.G., and Geyer, W.R. 2004. Turbulent energy production and entrainment at a highly stratified estuarine front. J. Geophys. Res. **109**(C5): C05004. doi:10.1029/2003JC002094.

Mackas, D.L., and Harrison, P.J. 1997. Nitrogenous nutrient sources and sinks in the Juan de Fuca Strait/Strait of Georgia/Puget Sound estuarine system: assessing the potential for eutrophication. Estuar. Coast. Shelf Sci. **44**(1): 1–21. doi:10.1006/ecss.1996.0110.

Masson, D., and Cummins, P.F. 2004. Observations and modeling of seasonal variability in the Straits of Georgia and Juan de Fuca. J. Mar. Res. **62**(4): 491–516. doi:10.1357/0022240041850075.

Ménesguen, A., Guillard, J.F., Aminot, A., and Hoch, T. 1995. Modeling the eutrophication process in a river plume — the Seine case-study (France). Ophelia, **42**: 206–225.

Parsons, T.R., Takahashi, M., and Hargrave, B. 1984. Biological oceanographic processes. Pergamon Press, New York.

Pawlowicz, R., Riche, O., and Halverson, M. 2007. The circulation and residence time of the Strait of Georgia using a simple mixing-box approach. Atmos.-ocean, **45**(4): 173–193. doi:10.3137/ao.450401.

Sastri, A.R., and Dower, J.F. 2009. Interannual variability in chitobiase-based production rates of the crustacean zooplankton community in the Strait of Georgia, British Columbia, Canada. Mar. Ecol. Prog. Ser. In press.

Spitz, Y.H., Newberger, P.A., and Allen, J.S. 2003. Ecosystem response to upwelling off the Oregon coast: behavior of three nitrogen-based models. J. Geophys. Res. **108**(C3): C03062. doi:10.1029/2001JC001181.

St. John, M.A., Marinone, S.G., Stronach, J., Harrison, P.J., Fyfe, J., and Beamish, R.J. 1993. A horizontally resolving physical–biological model of nitrate concentration and primary productivity in the Strait of Georgia. Can. J. Fish. Aquat. Sci. **50**: 1456–1466. doi:10.1139/f93-166.

Steele, J.H. 1962. Environmental control of photosynthesis in the sea. Limnol. Oceanogr. **7**: 137–150.

Sverdrup, H.U. 1953. On conditions for the vernal blooming of phytoplankton. J. Cons. Cons. Int. Explor. Mer, **18**: 287–295.

Thomson, R.E. 1994. Physical oceanography of the Strait of Geor-

gia – Puget Sound – Juan de Fuca Strait system. *In* Review of the marine environment and biota of the Strait of Georgia, Puget Sound, and Juan de Fuca Strait. *Edited by* R.C.H. Wilson, R.J. Beamish, F. Aitkens, and J. Bell. Can. Tech. Rep. Fish. Aquatic Sci. No. 1948. pp. 36–100.

Waite, A., Bienfang, P.K., and Harrison, P.J. 1992. Spring bloom sedimentation in a sub-arctic ecosystem. 1. Nutrient sensitivity. Mar. Biol. (Berl.), **114**: 119–129.

Yin, K., Harrison, P.J., Goldblatt, R.H., and Beamish, R.J. 1996. Spring bloom in the central Strait of Georgia: interactions of river discharge, winds and grazing. Mar. Ecol. Prog. Ser. **138**: 255–263. doi:10.3354/meps138255.

Yin, K., Goldblatt, R.H., Harrison, P.J., St. John, M.A., Clifford, P.J., and Beamish, R.J. 1997*a*. Importance of wind and river discharge in influencing nutrient dynamics and phytoplankton production in summer in the central Strait of Georgia. Mar. Ecol. Prog. Ser. **161**: 173–183. doi:10.3354/meps161173.

Yin, K., Harrison, P.J., Goldblatt, R.H., St. John, M.A., and Beamish, R.J. 1997*b*. Factors controlling the timing of the spring bloom in the Strait of Georgia estuary, British Columbia, Canada. Can. J. Fish. Aquat. Sci. **54**: 1985–1995. doi:10.1139/cjfas-54-9-1985.

Appendix A

The 46 CTD profiles from each of stations S2-2 and S3 (Fig. 1) from the surface to depth $D = -40$ m were fitted to similarity solution (see Batchelor 1967) for the cumulative freshwater, where the cumulative freshwater is defined as

$$(A1) \qquad F_{\mathrm{cum}}(z) = \int_D^z (S_D - S)\,\mathrm{d}z'$$

where $S_D = 30$ is the deep-water salinity, $S(z)$ is the salinity at depth z, and z is the vertical distance measured upward from the sea surface so that all values of z are negative. The similarity solution has two parameters: F, the surface value of the cumulative freshwater, and d, the depth at which F_{cum} is 67% of the surface value. Each of the two parameters was fitted to the data assuming a separable fit to the total freshwater Q_T and the distance r from the mouth of the Fraser River (taken here to be Sandheads). That the cumulative freshwater fit has the same form at stations S2-2 and S3 supports this relationship. So

$$(A2a) \qquad F_{\mathrm{cum}} = F\mathcal{F}\left(\frac{z}{d}\right)$$

$$(A2b) \qquad F = F_*\mathcal{F}_r\left(\frac{r}{r_3}\right)\mathcal{F}_T\left(\frac{Q_T}{\bar{Q}_T}\right)$$

$$(A2c) \qquad d = d_*\mathcal{D}_r\left(\frac{r}{r_3}\right)\mathcal{D}_T\left(\frac{Q_T}{\bar{Q}_T}\right)$$

where $F_* = 57.6$ m, $r_3 = 21.4$ km is the distance to station S3, $\overline{Q}_T = 3231$ m^3·s^{-1} is the mean total freshwater, $d_* = 11.7$ m, and $\mathcal{F}$ is a fitted polynomial function from the surface to the bottom of the plume at $2.5d$.

Consider quasi-steady Knudsen relations for conservation of mass and salt from the river mouth to some position r where we assume that the plume spreads as r^β with $\beta = 1.2$ (following Hetland and MacDonald 2008) and forms a fraction $c \approx 1/3$ of a circle at station S3. Then

$$(A3) \qquad S_D Q_T = 2\pi c r \int_{2.5d}^{0} V(S_D - S)\mathrm{d}z$$

where V is the radial velocity, also assumed to be a separable function of Q_T and r. Balancing the variation with respect to Q_T on the two sides of eq. A3 gives

$$(A4) \qquad V \propto \frac{Q_T}{\mathcal{F}_T}$$

and from conservation of mass, the upwelling velocity must be

$$(A5) \qquad w \propto \frac{Q_T \mathcal{D}_T}{\mathcal{F}_T}$$

Fitting $\mathcal{D}_T/\mathcal{F}_T$ to Q_T gives the second term in eq. 4.

Assuming that the pressure is hydrostatic and that pressure gradients are small at depth, the pressure gradient directed away from the mouth of the river can be directly calculated from the cumulative freshwater. This pressure gradient is large enough that it can be balanced only by turbulent momentum mixing. We assume a parabolic eddy viscosity profile, consistent with the KPP eddy viscosity profile and with observations near the mouth of the Fraser River (MacDonald and Geyer 2004). For mean river flow and at station S3, we assume a minimum eddy viscosity at the surface and at $2.5d$ of 8×10^{-4} m^2·s^{-1} and a maximum (at $1.25d$) of 4 to 6.5×10^{-3} m^2·s^{-1}. From this balance and estimating the spatial derivatives using differences between stations S2-2 and S3, the vertical profile of the horizontal velocity can be found. Conservation of mass then gives the vertical profile of the vertical velocity, which fits closely to the third term in eq. 4.

The value for w_* was found using eq. A3, estimating the integral using the vertical profile found from the pressure–turbulent mixing balance, taking $c = 1/3$ and, because the absolute value of the freshwater flux was needed, correcting Q_T for flow into the Fraser River after Hope (a factor of 1.66; Pawlowicz et al. 2007).

References

Batchelor, G.K. 1967. An introduction to fluid dynamics. Cambridge University Press, Cambridge, UK.

Hetland, R.D., and MacDonald, D.G. 2008. Spreading in the near-field Merrimack River plume. Ocean Model. **21**(1-2): 12–21. doi:10.1016/j.ocemod.2007.11.001.

MacDonald, D.G., and Geyer, W.R. 2004. Turbulent energy production and entrainment at a highly stratified estuarine front. J. Geophys. Res. **109**(C5): C05004. doi:10.1029/2003JC002094.

Pawlowicz, R., Riche, O., and Halverson, M. 2007. The circulation and residence time of the Strait of Georgia using a simple mixing-box approach. Atmos.-ocean, **45**(4): 173–193. doi:10.3137/ao.450401.